

Development and Biological Evaluation of Potent and Selective c-KIT^{D816V} Inhibitors

Soyoung Lee,^{†,‡} Hyunseung Lee,[§] Jinhee Kim,^{†,‡} Suhyun Lee,^{†,‡} Soo Jung Kim,[§] Byong-Seok Choi,[†] Soon-Sun Hong,^{*,§} and Sungwoo Hong^{*,‡,†}

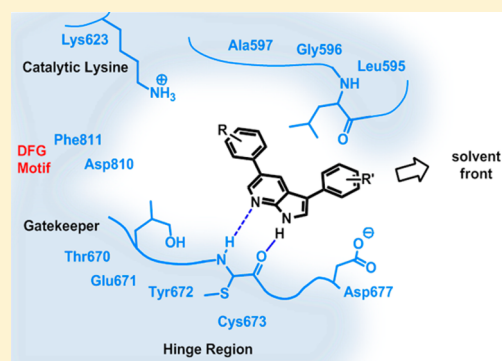
[†]Department of Chemistry, Korea Advanced Institute of Science and Technology (KAIST), Yuseong-gu, E6-4, Daejeon 305-701, Korea

[‡]Center for Catalytic Hydrocarbon Functionalizations, Institute for Basic Science (IBS), Daejeon 305-701, Korea

[§]Department of Biomedical Sciences, College of Medicine, Inha University, Incheon, 400-712, Korea

S Supporting Information

ABSTRACT: The c-KIT tyrosine kinase has emerged as a potential therapeutic target for an array of diseases. However, there exists a drug resistance that is caused by mutations in c-KIT; therefore, c-KIT remains as a clinical challenge due to limited effective treatment options for therapies. For example, the acquired activating point mutation D816V significantly impairs the efficacy of targeted cancer therapies. Understanding the mechanisms of drug resistance at the molecular level will aid in designing and developing particular inhibitors with the potential to overcome these resistance mutations. We undertake a structure-based de novo design of 7-azaindole as the molecular core using the modified scoring function. This approach led to an identification of new c-KIT inhibitors over 100-fold specific for the D816V mutant relative to the wild-type c-KIT with nanomolar inhibitory activity. More importantly, these compounds potently inhibit clinically relevant D816V mutations of c-KIT in biochemical and cellular studies.



INTRODUCTION

The c-KIT tyrosine kinase belongs to a family of type III receptor tyrosine kinase and is a transmembrane receptor that mediates the pleiotropic biological effects through its ligand stem cell factor (SCF, also known as mast cell growth factor).¹ Once SCF binds to an extracellular immunoglobulin-like domain of c-KIT, two monomeric c-KIT receptors become dimerized, resulting in an activation of downstream intracellular signal transduction, including phosphatidylinositol-3-kinase (PI3K)/Akt pathway, mitogen-activated protein kinase (MAPK), and signal transducer and activator of transcription (STAT), which are involved in cell proliferation, differentiation, and survival.^{2,3} Deregulated c-KIT kinase activity can be variably detected in multiple different types of pathogenesis, including small cell lung carcinoma, acute myeloid leukemia (AML), neuroblastoma, malignant melanomas, colorectal cancer, systemic mastocytosis (SM), and gastrointestinal stromal tumors (GISTs).^{3,4} The activation loop of the wild-type c-KIT exists in a dynamic equilibrium between the active and inactive conformations. Impairing c-KIT activity with tyrosine kinase inhibitors, such as imatinib, has yielded good responses in some c-KIT-dependent cancers.^{5,6} Imatinib is effective against the wild-type c-KIT by stabilizing the inactive conformation of the c-KIT kinase domain and then preventing the inactive form from switching to the active conformation of c-KIT.^{5,7}

Chemotherapy of cancers with first-line drugs often leads to resistance of the cancers.^{5,8} Gain-of-function point mutations in the c-KIT kinase domain result in a ligand-independent constitutive activation of c-KIT signaling, which leads to an uncontrolled mast cell proliferation and apoptosis resistance.^{9–11} Systemic mastocytosis patients have a gain-of-function mutation (c-KIT^{D816V}) in many cases.^{9,12} Introduction of the D816V point mutation disrupts the inactive conformation and impedes the binding process of first-line drugs, including imatinib, to the ATP-binding site of c-KIT.¹³ To date, only a few multikinase inhibitors, such as dasatinib¹⁴ and ponatinib,¹⁵ sufficiently block the activity of c-KIT^{D816V}.

Simultaneously inhibiting off-targets can result in a target-related toxicity because many individual biological targets are involved in important cellular functions. In this way, many multikinase inhibitors in clinical use might lead to possible side effects because off-target kinase inhibition can cause toxicity to normal cells.¹⁶ Recently, an interest has been growing in an effort to discover an approach to only inhibit the mutant therapeutic target, thereby minimizing the risk of potential side effects associated with the inhibition of normal function. The structural similarity has made the search for selective c-KIT^{D816V} inhibitors a challenging process. In this regard, it

Received: March 17, 2014

Published: July 8, 2014

would be worthwhile to identify *c*-KIT^{D816V} inhibitors in a specific manner over the wild-type *c*-KIT without normal SCF/*KIT* signaling pathway disruption. This strategy would potentially provide an effective treatment option as a special type of cancer treatment. Herein we describe our efforts to develop a new series of 7-azaindole-based inhibitors that may be effective and specific against *c*-KIT^{D816V} and demonstrate the biological activities of these compounds against imatinib-resistant HMC-1.2 cell lines.

RESULTS AND DISCUSSION

Identification of New *c*-KIT^{D816V} Inhibitors. We began our study by cross-screening our compound collection in search of *c*-KIT^{D816V} inhibitors. This led to an identification of a 7-azaindole-based derivative, combined with 3,4-dimethoxybenzene group at C3, and pyridylsulfonamide group at C5 as a *c*-KIT^{D816V} inhibitor (**1**, IC₅₀ = 346 nM) (Figure 1).¹⁷ The

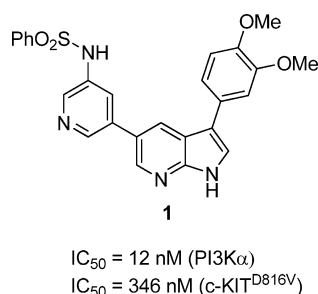


Figure 1. Initial hit for *c*-KIT^{D816V} inhibitors. Compounds were tested against *c*-KIT^{D816V} and PI3K α .

synthesized inhibitor compound **1** may impair *c*-KIT^{D816V} catalytic activity by specifically binding to the ATP binding site as illustrated in Figure 2. Because 7-azaindole scaffold has been used for PI3K α inhibitors,¹⁸ we proceeded to screen this series of compounds against PI3K α . Indeed, the newly identified *c*-KIT^{D816V} inhibitor **1** exhibited an inhibitory activity against PI3K α (IC₅₀ = 12 nM). Because the initial hit **1** was found to have a higher affinity for PI3K α , our first design efforts were focused on improving the selectivity against PI3K α while maintaining potent *c*-KIT^{D816V} inhibition.

The recent design of selective kinase inhibitors has been facilitated by the availability of substantial three-dimensional

structural information regarding various kinase–inhibitor complexes. The predicted hydrogen bonding network with Tyr836, Asp810, and the inhibitor in PI3K α (Figure 2A) was based on previous studies using X-ray crystallography.¹⁹ Our experience also confirmed the importance of a water-mediated hydrogen bond with residues in the active site of PI3K α .²⁰ Although hydrogen bonds appeared to form between pyridyl nitrogen at the 5 position of **1** and bound water molecule in PI3K, this key hydrogen bonding interaction was not expected in *c*-KIT^{D816V} (Figure 2B). We speculated that these structural differences can possibly provide a guideline for improving the selectivity via inhibitor modifications in this region of accessing specific spaces of the gatekeeper. With this agenda, our initial survey of the disruption of the key intermolecular hydrogen bonding network in PI3K α via C5 group modifications was conducted, probing the structural differences affecting the binding pockets of PI3K α and *c*-KIT^{D816V} (Figure 2).

Indeed, modification of the C5 group was essential for enhancing the selectivity over PI3K α , as shown in Table 1. Of particular significance was the observation that the binding affinity of **2** over PI3K α was dramatically reduced (IC₅₀ = 1.6 μ M for PI3K α) when the pyridyl group at the C5 position was replaced with a phenyl group, probably due to the disruption of the key hydrogen bond with a bound water molecule in PI3K α . We also noted that the sulfonyl group of aniline at the C5 position was allocated to generate further stabilizing interactions through the formation of hydrogen bond with Lys802 in PI3K α . With the binding mode set in this way, the sulfonyl group appeared to be unnecessary for producing an inhibitory activity over *c*-KIT^{D816V}. To verify this assumption, we then removed the sulfonyl group and assessed their inhibitory potencies over PI3K α and *c*-KIT^{D816V}. Subsequently, compound **4** exhibited excellent selectivity over PI3K α while retaining the lowest POC number for *c*-KIT^{D816V} (IC₅₀ = 6.3 nM for *c*-KIT^{D816V}, IC₅₀ > 10000 nM for PI3K α). Compound **3** was prepared as the control to investigate the role of the pyridyl group. Next, a second set of data was obtained for compounds in which C-5 aryl ring was substituted with a variety of patterns of groups. From these results, it was evident that either a removal of the sulfonamide group or a replacement of the pyridyl group with a phenyl group at C5 led to a dramatic loss in the inhibitory activity over PI3K α . Remarkably, this strategy has served well without compromising the *c*-KIT^{D816V} affinity, and most of 3,4-dimethoxybenzene derivatized compounds are

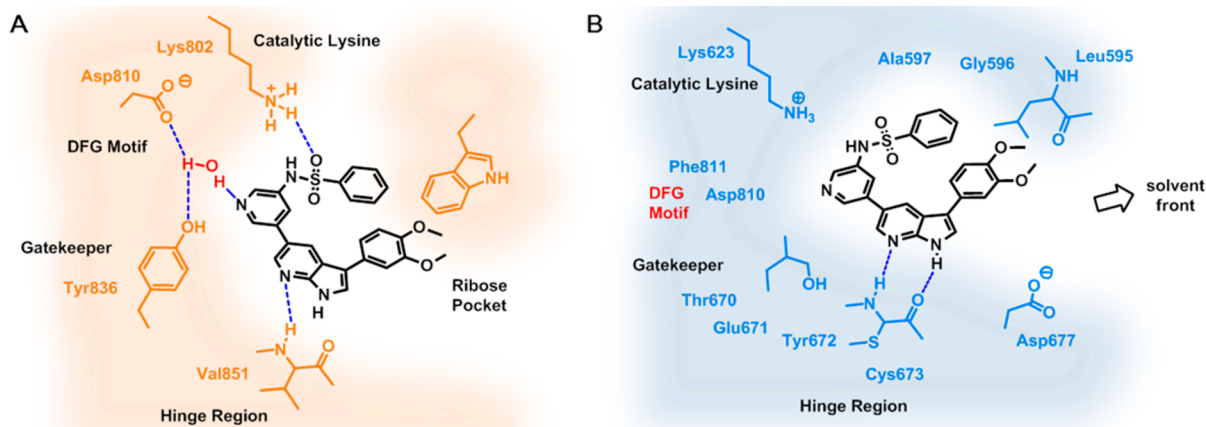
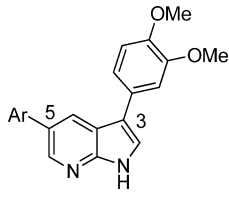


Figure 2. Design of new scaffolds as *c*-KIT^{D816V} inhibitors and opportunities for modification in the schematic active site of *c*-KIT^{D816V}. (A) Predicted binding mode of **1** in PI3K α . (B) Predicted binding mode of **1** in *c*-KIT^{D816V}.

Table 1. Exploration of Groups at the C5 Position of Azaindole Core^a



Compd	Ar	IC ₅₀ (nM)		Compd	Ar	IC ₅₀ (nM)	
		c-KIT (D816V)	PI3K α			c-KIT (D816V)	PI3K α
1		346	12	11		60.1	>10,000
2		125.8	1,600	12		785	>10,000
3		10.8	1,450	13		1330	>10,000
4		6.3	>10,000	14		426	>10,000
5		63.8	>10,000	15		72.8	>10,000
6		29.2	>10,000	16		457	>10,000
7		261.4	>10,000	17		571.3	>10,000
8		520	>10,000	18		32.1	>10,000
9		134.6	>10,000	19		2.1	>10,000
10		32.1	9,700	20		102	>10,000

^aCompounds were tested against c-KIT^{D816V} and PI3K α .

found to have a greater binding affinity for c-KIT^{D816V} than PI3K α (Table 1). We also examined the significance of the *meta*-substituents at the C5-aryl ring and observed that the binding affinity for c-KIT^{D816V} was dramatically reduced when the *meta*-amino group of compound 4 was moved to the *ortho*-position (13).

De Novo Design. On the basis of the preliminary data, compound 4 was selected as an initial hit compound to allow for additional interactions to be identified. We explored the space at 3- and 5- positions of 7-azaindole to identify the derivatives with enhanced potency through the structure-based de novo design, as summarized in Figure 3. Thus, we prepared two receptor models to perform the de novo design of 7-

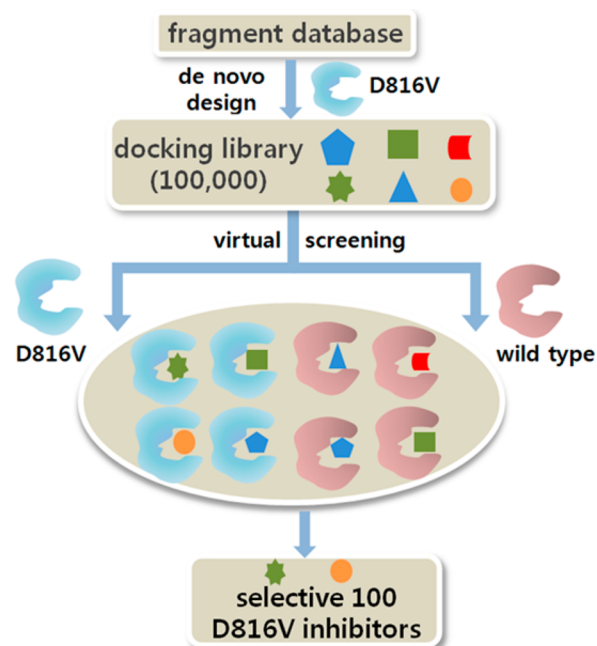
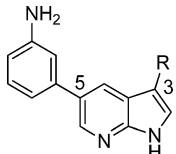


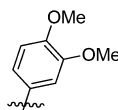
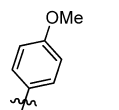
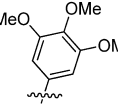
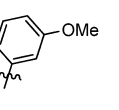
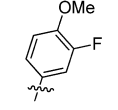
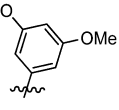
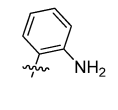
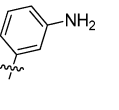
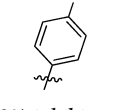
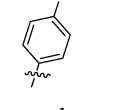
Figure 3. Flowchart for the discovery process of potent and selective inhibitors of D816V mutant of c-KIT through the structure-based de novo design.

azaindole derivatives: one is the homology modeling for the structure of c-KIT^{D816V} constructed by the MODELER program on the basis of wild-type c-KIT in the active conformation,^{21,22} and the other is the autoinhibited form of the wild-type (PDB entry: 1T45)²³ as for the wild-type c-KIT model. First, a variety of 7-azaindole derivatives were generated with the LigBuilder program²⁴ based on the structure of the D816V mutant–azaindole complex obtained from docking simulations. To score the generated derivatives with consideration of their binding affinity for c-KIT and c-KIT^{D816V}, the program employed an empirical binding free energy function.²⁵ As the starting point for generating 7-azaindole derivatives, we analyzed the binding pocket in the ATP-binding site of the D816V mutant using the POCKET module. The structure of c-KIT^{D816V} in complex with 7-azaindole was used as the input to identify key interacting residues in the ATP-binding site. From this information, it could be possible to define a binding model of 7-azaindole inhibitors at the ATP binding site. A variety of 7-azaindole derivatives were then generated via an application of genetic algorithm, whereby the structures evolved as the chemical groups modified at the substitution positions of the 7-azaindole core, and these derivatives were rescored with the modified scoring function (see the Supporting Information). The generated 7-azaindole derivatives were then selected according to the calculated binding free energy to maximize the affinity for the D816V mutant and minimize the affinity for wild-type c-KIT.

The de novo design studies identified a variety of functional groups to introduce the 7-azaindole core at the 3- and 5- positions. For the synthesized derivatives, IC₅₀ (50% inhibitory concentration) values were determined against the wild-type c-KIT and D816V mutant.²⁶ To determine whether or not the 3,4-dimethoxy phenyl group at the C3 position of initial hit 4 was optimal, the effects of its replacement with other groups were explored, and a series of (hetero)aryl groups were installed (Table 2). Because the 3-aniline group at the C5

Table 2. Exploration of Groups at the C3 Position of Azaindole Core^a



Compd	Ar	c-KIT (D816V) IC ₅₀ (nM)	Compd	Ar	c-KIT (D816V) IC ₅₀ (nM)
4		6.3	25		398
21		97.7	26		670
22		104	27		320
23		1420	28		76.7
24		>10,000	29		2260

^aIC₅₀ (50% inhibitory concentration) values were determined against the D816V mutant.

position of **4** proved to be effective for high inhibitory activity, we tentatively fixed the 3-aniline group in this region, then screened various groups at the C3 position. We observed that the binding affinity and potency were reduced when the 3,4-dimethoxy group was replaced with the 3,5-dimethoxy group (**27**) or the monomethoxy group (**25** and **26**), indicating that the orientation of the dimethoxy group is critical in sustaining potency. The enzyme potency of the derivatives was also decreased when the trimethoxy group was introduced (**21**), demonstrating that the 3,4-dimethoxy phenyl group at the C3 position group is the maximum size that is suitable for this position in the 7-azaindole core. A comparison of the IC₅₀ values of **4** (IC₅₀ = 6.3 nM) to that of **22** (IC₅₀ = 104 nM) clearly reveals that substitutions of other chemical groups for the 3,4-dimethoxybenzene moiety lead to a large decrease in the inhibitory activity against c-KIT^{D816V}. From the first round of C3 array exploration, derivatives bearing 3,4-dimethoxybenzene appeared to be the superior inhibitors, suggesting that this group is an effective substituent for the potent activity against c-KIT^{D816V}.

Enhancement of Selectivity for the D816V mutant.

The aniline **4** proved to be a potent c-KIT^{D816V} inhibitor (IC₅₀ = 6.3 nM) and represented a potent hit in our c-KIT^{D816V} program. To address the structural and mechanistic aspects that are relevant to the selective inhibition of the D816V mutant by these newly identified inhibitors, we carried out docking studies for c-KIT^{D816V} in complex with **4**. Previous molecular modeling

and dynamics simulation studies revealed that the activating D816V mutation triggers spontaneous detachment of the juxtamembrane domain from the c-KIT domain, which stabilizes the activation loop (A-loop) in the extended conformation.²¹ This conformational change in c-KIT^{D816V} results in maintaining the active form, which enables constitutive oncogenic activation. Figure 4 displays representative MD trajectory snapshots of the D816V mutant–**4** complexes. The binding modes of **4** with the D816V mutant shows that the 7-azaindole skeleton fully maintains the bidentate hydrogen bonding pattern with the backbone groups of Cys673, which reveal that the strengths and dynamic stabilities of the bidentate hydrogen bonds with Cys673 serve as critical factors that affect the potency and selectivity of c-KIT^{D816V} inhibitors. Compound **4** appears to be stabilized through the hydrophobic interactions with side chains Leu595, Val603, Ala621, Tyr672, and Leu799. Another feature in the binding modes of **4** is that the terminal 3,4-dimethoxybenzene group appears to be exposed to the bulk solvent in the c-KIT–**4** complex and stabilized through interactions with the protein groups at the entrance of the ATP-binding site of c-KIT^{D816V}.

Having identified the significance of the 3,4-dimethoxyphenyl group at the C3 position of 7-azaindole, we carried out a broader exploration of analogues which incorporated this key functional group (Table 3). In general, the synthesized derivatives appear to maintain the bidentate hydrogen bonding with the backbone groups of Cys673 in both c-KIT and c-KIT^{D816V}. The aromatic ring system of these analogues is further stabilized through hydrophobic interactions with nonpolar residues, including Leu595, Val603, Ala621, Leu799, Tyr672, and Cys674. The third hydrogen bond in the P-loop appears to be established in a different fashion in complex of wild-type c-KIT and the D816V mutant. The molecular modeling study indicated that Asp-Phe-Gly (D810-F8111-G812) motif in the A-loop and the glycine-rich phosphate-binding loop (P-loop) form a deep hydrophobic pocket in c-KIT^{D816V}. In contrast, the p-loop in the wild-type is away from 7-azaindole, as shown in Figure 4B. The 3-aminophenyl group at C5 faced into the hydrophobic pocket constructed by phosphate-binding loop and activation loop in the ATP-binding sites of c-KIT^{D816V}. This suggests that there exists a possibility of further elaboration of the substituents of C5 aryl ring (Figure 4).

With this agenda, a diverse set of substituents were investigated to expand the structure–activity relationship, and the analogues incorporated an additional substituent into the 3-aminophenyl group in order to enhance the selectivity for c-KIT^{D816V}. In this series of analogues, it appeared that the presence of an additional substituent on the 3-aniline ring was generally tolerant to its function on c-KIT^{D816V}. In contrast, the potency on the wild-type c-KIT was tunable by modification of the substitution patterns of the C5-aryl ring as seen in Table 3. The relatively low potency for wild-type c-KIT of 7-azaindole inhibitors with a larger group substituted 5-aryl ring may be rationalized by the decreased volume of the ATP-binding pocket in wild-type c-KIT due to the approach of JMR residues to the gatekeeper site in the inactive conformation. The substitution patterns of C5 aryl ring also proved to be an important structural requirement for the design of c-KIT^{D816V} selective inhibitors. Thus, introduction of an additional methoxy group at the *para*-position of the 3-aniline ring (**34**) resulted in highly amplified selectivity vs wild-type c-KIT (IC₅₀ >10000 nM for c-KIT, IC₅₀ = 25.6 nM for c-KIT^{D816V}). In the

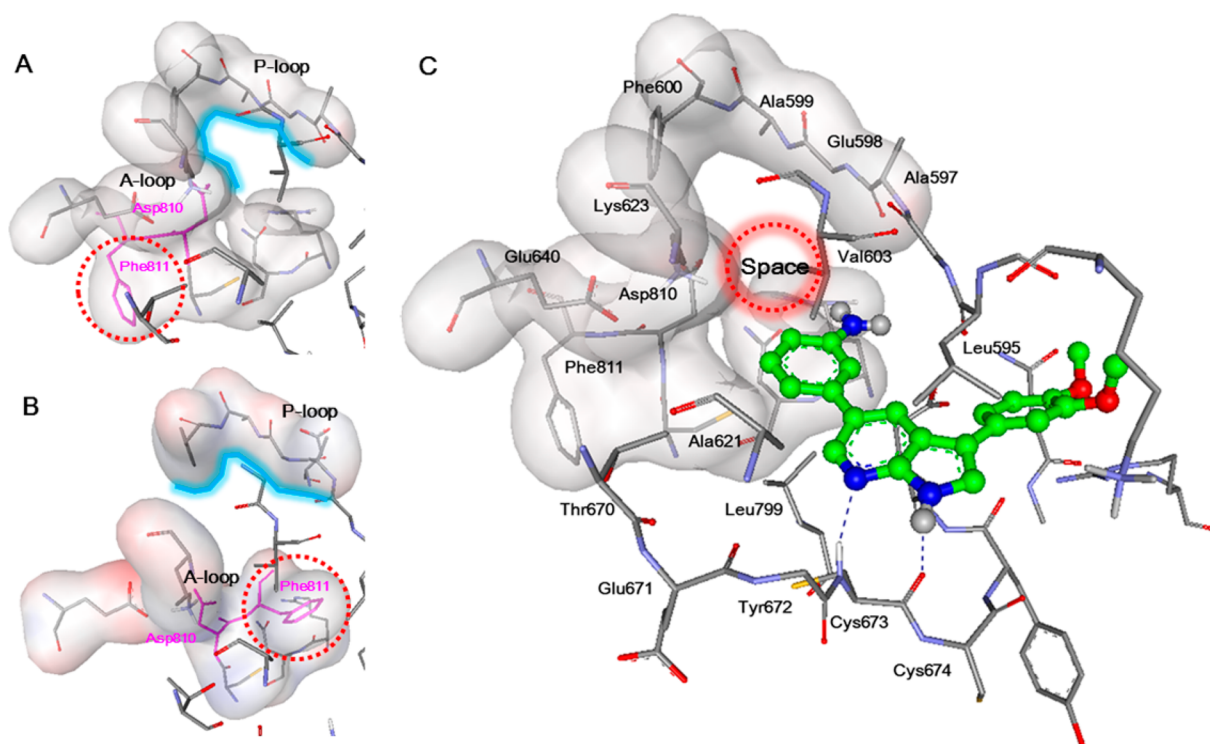


Figure 4. Representative MD trajectory snapshots of the hydrophobic pocket constructed by phosphate-binding loop and activation loop in the ATP-binding sites of (A) c-KIT^{D816V} and (B) wild-type c-KIT. (C) Predicted binding mode of **4** with the D816V mutant of c-KIT. Carbon atoms of c-KIT and **4** are indicated in gray and green, respectively. Asp810 and Phe811 of DFG motif are indicated in magenta. Each navy dotted line indicates a hydrogen bond.

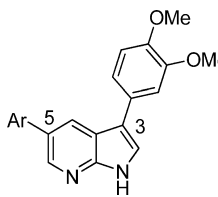
D816V mutant, both substituents at the *meta*- and *para*-position of C5 aryl ring of compound **34** are expected to extend the P-loop and make favorable contacts with backbone groups of residues in the pocket (Figure 5A). In addition, the methoxy group at the *para*-position appeared to establish an additional hydrogen bond with the side-chain amino group of Lys623. By contrast, this binding mode cannot be formed in the c-KIT–**34** complex because the P-loop is too distant from the ATP-binding site, and accessing to the extended P-loop is prevented by Phe811 in the wild-type c-KIT. Instead, it is observed that the C5 aryl ring points toward a small hydrophobic pocket formed by the side chains of Ile699, Thr670, Val622, Leu644, and Lys623–Glu640 salt bridge in the wild-type (Figure 5B). This hydrophobic region is too small to comfortably accommodate the two substituents coming off the C5 aryl ring, and unfavorable steric contacts would be present in the wild-type c-KIT. The structural comparison of c-KIT and c-KIT^{D816V} in the P-loop revealed that the interaction of 7-azaindole with hydrophobic pocket in the P-loop could serve a key structural determinant of the specificity of the D816V mutant selective inhibitors.

Because these structural differences provided a guideline toward favorable impact on selectivity improvement for the D816V mutant, several other groups were designed to extend the substituent at this region (Table 3). The preference of *meta*- and *para*-substituents of C5-aryl ring for the enhancement of selectivity for c-KIT^{D816V} is further illustrated by the potency of analogue **31** bearing in the form of a morpholinoacetyl group ($IC_{50} = 9140$ nM for c-KIT, $IC_{50} = 8.5$ nM for c-KIT^{D816V}). The inhibitory activity was also increased over the D816V mutant when the methoxy group was replaced with a 2-morpholinoethoxy appendage (**40**, $IC_{50} = 13.9$ nM) while

retaining excellent selectivity over the wild-type c-KIT. The 3,4,5-trimethoxy aryl group was also tolerable to the D816V mutant, and **32** ($IC_{50} = 8.8$ nM) was more potent than the corresponding 4-methoxy derivative **18** ($IC_{50} = 32.1$ nM) and 3-methoxy derivative **41** ($IC_{50} = 28.7$ nM). Methyl substitution (**33**) had no appreciable change on both the wild-type c-KIT and the D816V mutant when compared with the corresponding **34**. Intriguingly, replacement of the 3-NH₂ group of **34** with a 3-OMe group (**19**) resulted in about 10-fold increase in potency on the D816V mutant ($IC_{50} = 2.1$ nM). Attempts to further increase potency by linking or repositioning substituents of C5-aryl ring (**35**, **36**, and **39**) were unremarkable, and no compound offered any advantage relative to the corresponding compound **19**. Cumulatively, these results indicate that disubstitution at the *meta*- and *para*-position of C5 aryl ring in this series was most effective for achieving high selectivity for the D816V mutant.

Interestingly, moving the substituent from the *meta*- to the *para*-position of C5 aryl ring led to increase in the inhibitory activity against the wild-type c-KIT, thus reducing the selectivity for the D816V mutant (**18**, **37**, and **38**). For example, changing the substituent from 3-aminobenzene in **4** to 4-aminobenzene in **37** led to almost a 20-fold increase in the inhibitory activity against the wild-type c-KIT ($IC_{50} = 56.8$ nM) but only a slight change in the IC_{50} values with respect to the D816V mutant ($IC_{50} = 9.1$ nM). Compound **18** bearing a 4-methoxy group at the *para*-position also showed a decrease in selectivity for the D816V mutant. When the *para*-amino group in compound **37** was replaced by the methyl group in compound **17**, it resulted in a substantial loss of activity on both the wild-type c-KIT ($IC_{50} > 10\,000$ nM) and the D816V mutant ($IC_{50} = 571.3$ nM). Because moving the substituent

Table 3. Influence of C5 Groups on Selectivity



Compd	Ar	IC ₅₀ (nM)		Compd	Ar	IC ₅₀ (nM)	
		WT	D816V			WT	D816V
4		1064	6.3	33		>10,000	24.6
5		>10,000	63.8	34		>10,000	25.6
11		3330	60.1	35		10,800	48.8
17		>10,000	571.3	36		5460	29.2
18		371	32.1	37		56.8	9.1
19		142.0	2.1	38		1290	67.8
30		1160	65.1	39		>10,000	26.2
31		9140	8.5	40		8540	13.9
32		2754	8.8	41		1520	28.7

from the *meta*- to the *para*-position of C5 aryl ring resulted in an increased potency over the wild-type, the binding mode of **37** was further analyzed with MD simulations.

The binding modes of **37** in the ATP-binding sites of the wild-type c-KIT and the D816V mutant, obtained from energy minimizations of the time-averaged structures of c-KIT–**37** and D816V–**37** complexes, are compared in Figure 6. With regard to the structure, **37** is stabilized through bidentate hydrogen bonds between 7-azaindole ring and Cys673, hydrophobic interactions of aromatic rings with nonpolar residues, and a hydrogen bond between the NH₂ group and the backbone aminocarbonyl oxygen of Asp810. Despite the overall similarity in the binding modes of **4** and **37** toward the wild-type c-KIT, some differences in inhibitor positions with respect to the ATP-

binding site and the P-loop are also observed in the wild-type–**37** complexes. For example, the inhibitor moves from the activation loop to the ATP-binding site (residues 670–677) in the c-KIT–**37** complex, establishing a hydrogen bond between the 4-aniline group of **37** and the backbone aminocarbonyl oxygen of Asp810 (Figure 6B). This positional shift strengthens the bidentate hydrogen bonds between 7-azaindole ring and Cys673. The average N···H–N and N–H···O hydrogen bond distances are 1.82 and 1.78 Å, respectively, in c-KIT–**37** complex. The approach of **37** to the ATP-binding may also have an effect in promoting van der Waals interactions between the 7-azaindole group and the side chains of Val654, Tyr672, and Leu799 (Figure 6B). Therefore, the strengthening of the hydrogen bonds with the backbone groups of Asp810 and

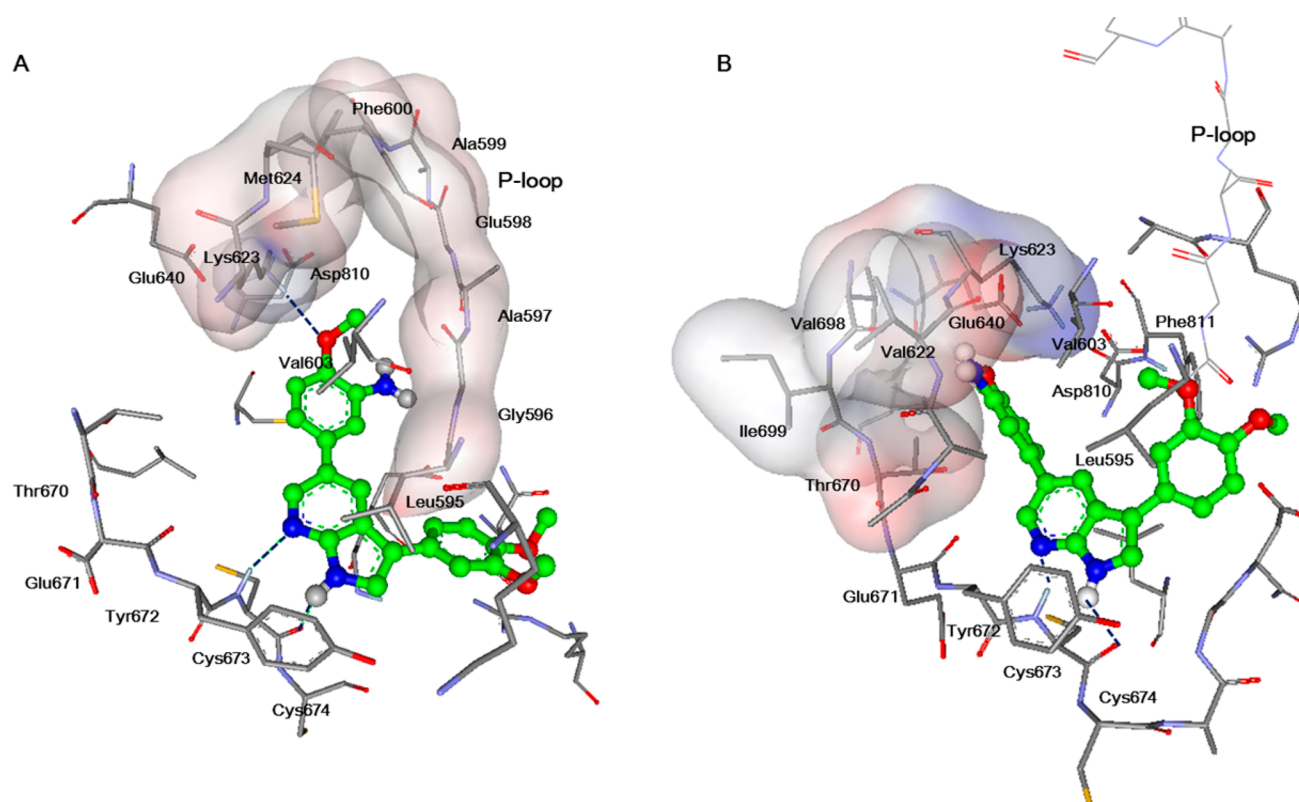


Figure 5. (A) Predicted binding mode of 34 with c-KIT^{D816V} and (B) with wild-type c-KIT. Each navy dotted line indicates a hydrogen bond.

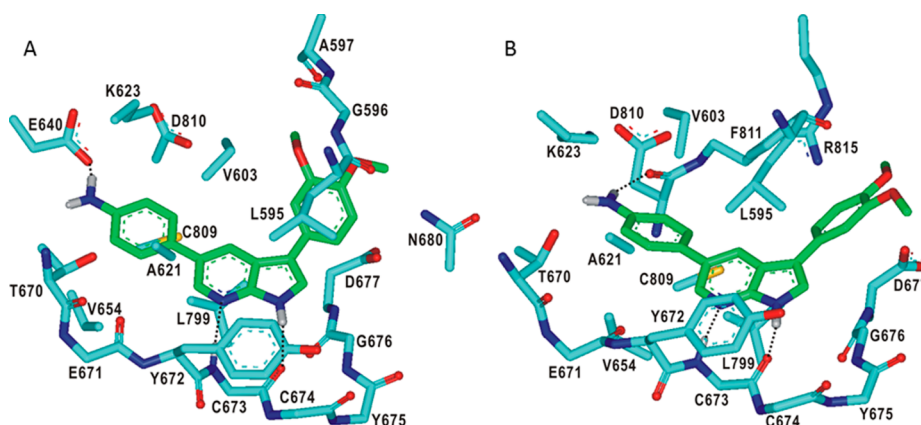


Figure 6. Representative MD trajectory snapshots of 37 in the ATP-binding sites of (A) c-KIT^{D816V} and (B) wild-type. Carbon atoms of c-KIT and 37 are indicated in cyan and green, respectively. Each dotted line indicates a hydrogen bond.

Cys673, as well as hydrophobic interactions with nonpolar residues around the ATP-binding site, may contribute to the potent inhibitory activity of 37 with respect to the wild-type c-KIT. The binding mode of 37 for the D816V mutant differs from that of the wild-type in that the role of the hydrogen bond acceptor with respect to the terminal aniline moiety is played by a side chain carboxylate ion of Glu640 instead of the backbone aminocarbonyl oxygen of Asp810 (Figure 6A). The above modeling analysis similarly applies to compound 18, leading to an increased potency over the wild-type c-KIT. The loss of hydrogen bond interactions between derivative 17 bearing C5 *p*-tolyl group and the backbone aminocarbonyl oxygen of Asp810 may explain the substantial loss of activity on the wild-type c-KIT ($IC_{50} > 10000$ nM).

Kinase Selectivity Profiling. To obtain the detailed picture of selectivity profile of this series, potent inhibitors were subjected to kinase selectivity profiling with a panel of 48 cancer related kinases, representing major branches (TK, TKL, STE, CMGC, CAMK, AGC, atypical, and other) on the kinome tree at 1 μ M concentrations in a high-throughput binding assay (Figure 7, KINOMEScan, Ambit Biosciences).²⁵ Overall, this series of inhibitors showed moderate to good specificity profiles relative to current multitargeted c-KIT^{D816V} inhibitors such as dasatinib and ponatinib; however, these inhibitors are less selective for the TK kinase family including FLT3, JAK2, TRKA, and TRKB. Other kinases inhibited by this series are DRAK1 (CAMK family), Aurora A, Aurora B, IKKa, and IKKb as shown in Figure 7 (see Supporting Information Table S1 for more details). Among this series of inhibitors,

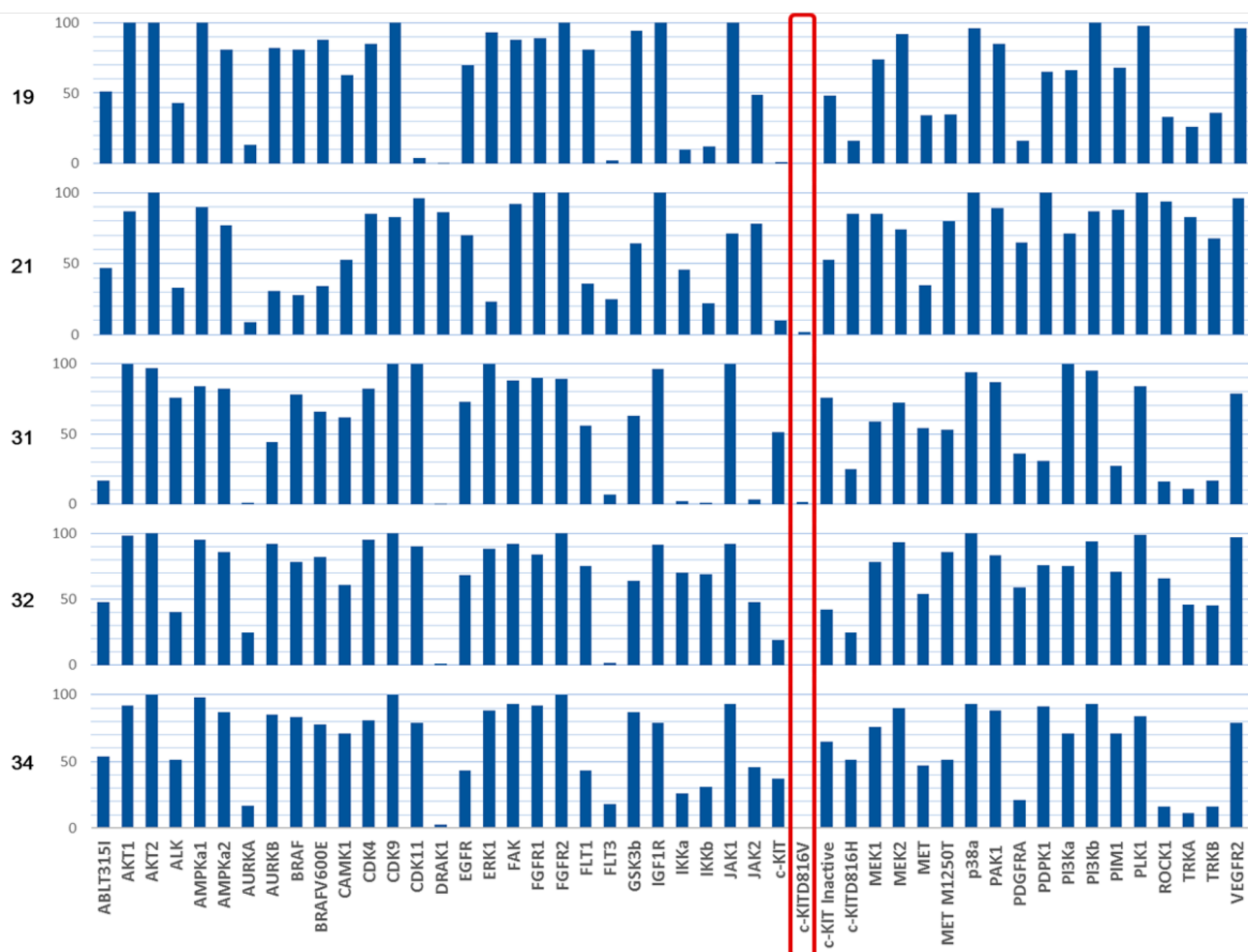


Figure 7. Selectivity profiles of compounds **19**, **21**, **31**, **32**, and **34**. A panel of 48 kinases was tested at 1 μM concentrations in a high-throughput binding assay (see Supporting Information for details).

trimethoxy derivative **32** exhibited an improved selectivity profile, and two kinases against which **32** demonstrated tight off-target binding affinity ($\text{IC}_{50} < 1 \mu\text{M}$) were FLT3, and DRAK1. On the other hand, compound **31** showed only modest specificity profiles against other kinases and displayed significant off-target activity over 10 kinases (ABL^{T315I}, Aurora A, DRAK1, FLT3, IKKa, IKKb, JAK2, ROCK1, TRKA, and TRKB).

Antiproliferation Activity. This series of potent inhibitors were further tested for cellular growth inhibition against human mast cells (Table 4). We carried out an evaluation of their antiproliferative activity on HMC-1.2 cell lines (V560G, D816V), which are imatinib-resistant. To measure the inhibitory effect of these compounds on cell growth, cell viability was tested by 3-(4,5-dimethylthiazol-2-yl)-2,5-diphenyltetrazolium bromide (MTT) assay in HMC-1.2 at various

concentrations for 48 h. Notably, compounds **19**, **21**, **32**, and **34** showed potent antiproliferative effects at submicromolar concentration as shown in Table 4. This series of compounds displayed significant off-target activity ($\text{IC}_{50} < 10 \mu\text{M}$) over several kinases (DRAK1, FLT3, and IKK) which are believed to be involved in cell proliferation. On the basis of the selectivity data, off-target activity might be partially responsible for potent antiproliferative effects. For example, DRAK1 and FLT3 displayed tight binding to this series of compounds (DRAK1 by **19**, **31**, **32**, **34**; FLT3 by **19**, **31**, and **32**). Compound **31** also exhibited significant activities over IKKa and IKKb.

A couple of cases of discordances were observed between IC_{50} values over c-KIT^{D816V} and cellular potencies, which may be attributed to the inability of the enzymatic assay data to accurately reflect the cell potencies. Because intracellular activity is influenced by the physicochemical properties of compounds, we further measured basic profiles of these compounds (see Table S5 in Supporting Information). The good ability of **21** and **34** to suppress the growth of HMC-1.2 cells might be attributable to their more desirable range of properties, whereas more potent compound **31** in the biochemical assay exhibited a lower AlogP value and higher topological polar surface area (tPSA). Likewise, compounds **19** and **32** showed a higher AlogP value and lower tPSA than **21** or **34**.

Table 4. Effect of C-KIT Inhibitors on Growth of HMC-1.2

compd	HMC-1.2 (V560G, D816V) IC_{50} (μM)	compd	HMC-1.2 (V560G, D816V) IC_{50} (μM)
imatinib	17	21	0.81
dasatinib	0.82	31	2.01
ponatinib	0.35	32	0.91
4	1.68	33	1.43
19	0.76	34	0.87

Cell-Signaling Effects. c-KIT signaling is transmitted through several pathways, including signal transducer and activator of transcription, and activation of the c-KIT pathway leads to the phosphorylation of STAT3, Akt, and Erk, a downstream effector of phosphatidylinositol 3-kinase. To ensure that the new series of compounds was inhibiting c-KIT-dependent downstream signaling pathways in HMC-1.2 cells, several potent inhibitors were further profiled for their ability to suppress cellular biomarkers, using Western immunoblotting. Consistent with the expectations for a potent c-KIT inhibitor, **19**, **21**, **32**, and **34** strongly suppressed the phosphorylation of STAT3, Akt, and Erk. We also compared the suppression of c-KIT signaling by these inhibitors with imatinib, dasatinib, and ponatinib as shown in Figure 8.

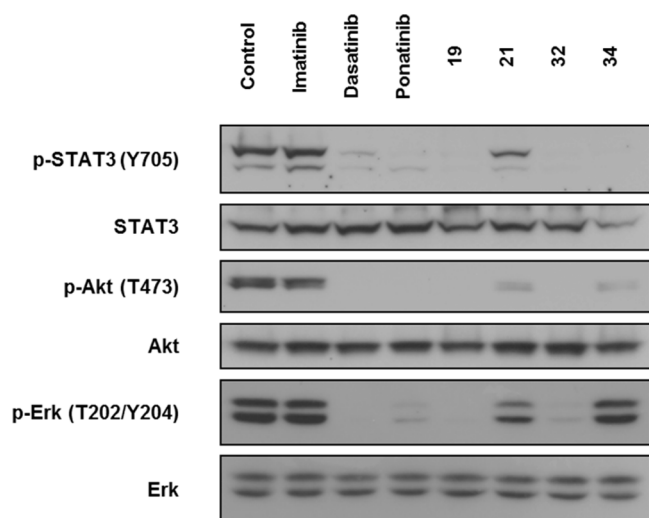


Figure 8. Inhibition of cellular c-KIT pathway including STAT3, Akt, and Erk in HMC-1.2 (imatinib-resistant human mast cell). HMC-1.2 cells were starved with serum-free IMEM for 2 h and treated with imatinib, dasatinib, ponatinib, **19**, **21**, **32**, and **34** for 1 h at 5 μ M.

Cell-Cycle Distribution and Apoptotic Cell Death. In general, cell apoptosis and growth correlate with the cell cycle progression. Blocking the kinase pathway can change the cell cycle distribution and promote apoptosis. Because compound **19** successfully demonstrated the ability to inhibit p-STAT3, p-Akt, and pErk in HMC-1.2 cells, we further determined whether the inhibition of c-KIT in HMC-1.2 cells by compound **19** induces a cell cycle arrest. The cell cycle distribution was evaluated by a flow cytometric analysis. The treatment of **19** inhibited the cell cycle progression in HMC-1.2 cells, resulting in a significant increase in the percentage of cells in the SubG1/G1 phase in a dose dependent manner (Figure 9).

We next analyzed the ability of **19** to induce apoptosis in HMC-1.2 cells. When HMC-1.2 cells were exposed to various doses of **19**, the DNA fragmentation, one of the hallmarks of apoptosis, was increased in a dose-dependent manner (Figure 10). A flow cytometric analysis of HMC-1.2 cells, which were subjected to terminal deoxynucleotidyl transferase-mediated nick end labeling (TUNEL) staining, revealed that the percentage of TUNEL-positive cells increased after treatment with **19**, further supporting the conclusion that **19** induced apoptosis.

Chemical Synthesis. The general synthesis of representative 3,5-disubstituted 7-azaindole derivatives **48** is shown in

Scheme 1. A two-step reaction sequence, starting from a known-compound **45**, was utilized to afford the desired derivative **48**. An initial Pd-catalyzed cross-coupling with C3 (hetero)aryl partners was carried out to afford a C3 aryl intermediate, which were then subjected to benzenesulfonyl group deprotection under basic conditions, resulting in compound **46**. An assortment of the C5 groups of 7-azaindole was then explored through another Suzuki coupling reaction with the appropriate arylboronic acids or esters, yielding focused set of target compounds. For focused C5-aryl group array, the key intermediate **47** was prepared via direct borylation of 5-bromoazaindole **46**. The corresponding desired compounds **48** were then obtained by Pd-catalyzed cross-coupling with the appropriate aryl boronic acids or esters.

CONCLUSION

The 7-azaindole-based hit **4** was modified by applying a structure-based de novo design to obtain new potent and selective inhibitors for the gain-of-function D816V mutant. The 7-azaindole derivatives with a 3,4-dimethoxybenzene moiety at the 3-position and a polar aromatic group at the 5-position were found to have a nanomolar inhibitory activity for the D816V mutant, with more than 100-fold greater potency compared to the wild-type c-KIT. A decomposition analysis of the binding free energies indicates that the potency of an inhibitor can be optimized by reducing desolvation cost for enzyme–inhibitor complexation as well as by strengthening the interactions between the inhibitor and c-KIT in the ATP-binding site. Four of the compounds suppress cell growth and proliferation against imatinib-resistant HMC-1.2 cell lines in a submicromolar concentration range. Compound **19** also induced apoptosis through regulation of the c-KIT signaling pathway, which leads to strong anticancer activity in HMC-1.2 cells. Future studies may be necessary to fully identify the potential of this series as a modality for cancer treatment.

EXPERIMENTAL SECTION

I. General Methods and Materials. Unless stated otherwise, reactions were performed in a flame-dried glassware under positive pressure of nitrogen using freshly distilled solvents. Analytical thin layer chromatography (TLC) was performed on precoated silica gel 60 F₂₅₄ plates, and visualization on TLC was achieved via UV light (254 and 354 nm). Flash column chromatography was utilized on silica gel (400–630 mesh). ¹H NMR was recorded on 600 or 400 or 300 MHz, and chemical shifts were quoted in parts per million (ppm) referenced to the appropriate solvent peak or 0.0 ppm for tetramethylsilane. The following abbreviations were used to describe the peak splitting patterns when appropriate: br = broad, s = singlet, d = doublet, t = triplet, q = quartet, m = multiplet, dd = doublet of doublet. Coupling constants, *J*, were reported in hertz unit (Hz). ¹³C NMR was recorded on 100 or 150 MHz and was fully decoupled by broad band proton decoupling. Chemical shifts were reported in ppm referenced to the center line of a triplet at 77.0 ppm of chloroform-*d*. Mass spectral data were obtained from the KAIST Basic Science Institute by Bruker Daltonik HR-MS using the EI method or Agilent LR-MS. High-performance liquid chromatography analyses for checking mass spectral data (using EI method) and the purity (>95% area) and of synthesized compounds were performed on a Agilent HPLC equipped with an Agilent Poroshell 120 EC-C18 reverse phase column (4.6 mm \times 50 mm, 2.7 μ m) and by quadrupole LC/MS. The mobile phase was a mixture of MeOH (0.1% TFA) and H₂O (0.1% TFA). Compound purity was determined by integrating the peak areas of liquid chromatogram, monitored at 254 nm. Flow rate (0.5 mL/min): Gradient system, from MeOH (0.1% TFA) 10% and H₂O (0.1% TFA) 90% (0 min) to MeOH (0.1% TFA) 90% and H₂O (0.1% TFA) 10%

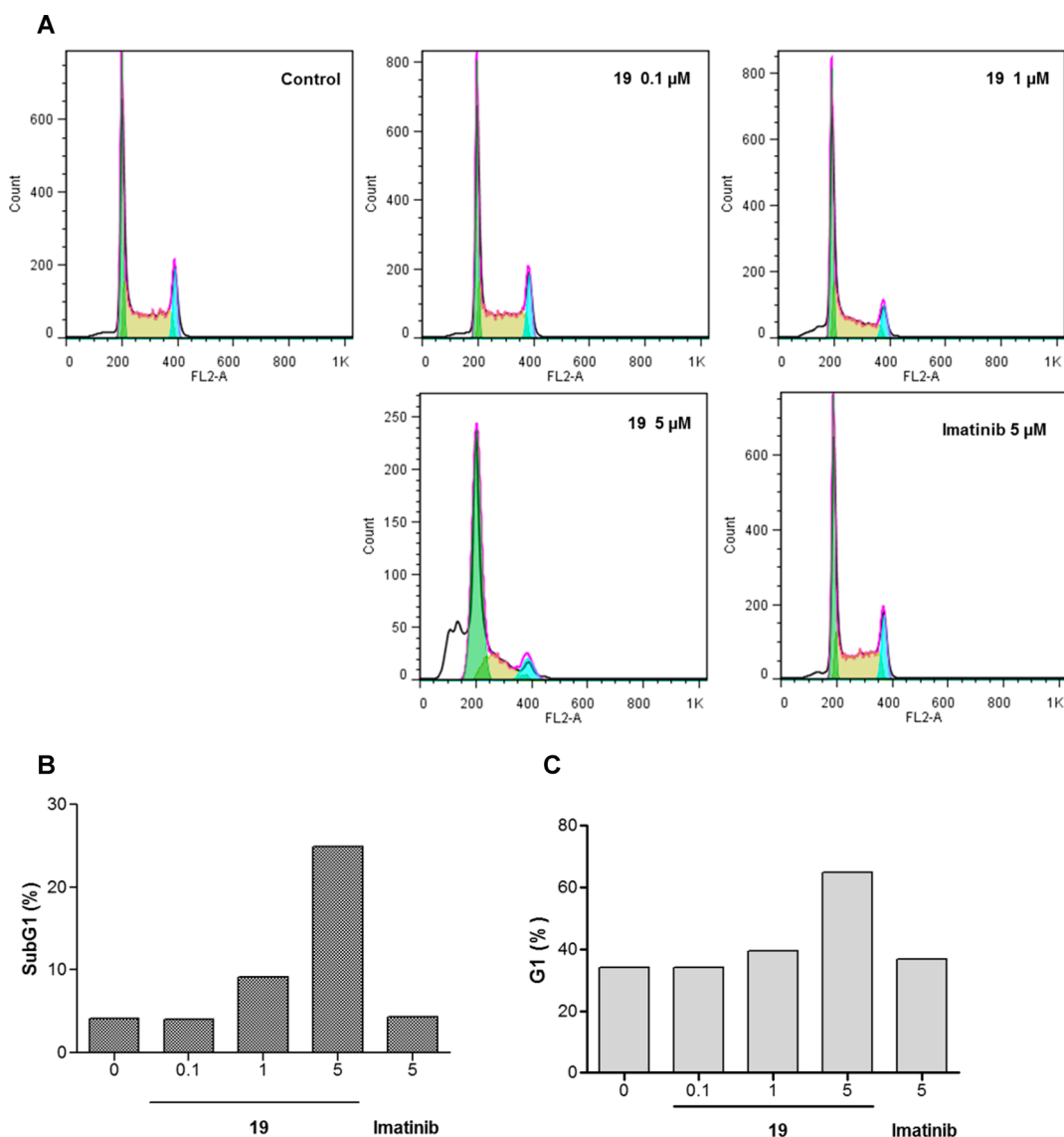


Figure 9. Effect of **19** on the cell cycle distribution. HMC-1.2 cells were exposed to increasing concentration of **19** and 5 μ M imatinib for 24 h. Compound **19** arrested the cell cycle at G1 phase in a dose-dependent manner.

(18 min), the solvent ratio was maintained for 23 min; the solvent ratio was changed to MeOH (0.1% TFA) 10% and H₂O (0.1% TFA) 90% (25 min). All final compounds were found to have >95% purity. Commercial grade reagents and solvents were used without further purification except as indicated below. Dichloromethane was distilled from calcium hydride. THF was distilled from sodium.

II. Preparation of Compounds. General Procedure (GP I) for Suzuki Coupling. 5-Bromo-3-(3,4-dimethoxyphenyl)-1H-pyrrolo[2,3-*b*]pyridine (**46**). A solution of 5-bromo-3-iodo-1-(phenylsulfonyl)-1H-pyrrolo[2,3-*b*]pyridine (600 mg, 1.3 mmol), 3,4-dimethoxyphenylboronic acid (284 mg, 1.56 mmol), Cs₂CO₃ (1060 mg, 3.25 mmol), and PdCl₂(dppf)·CH₂Cl₂ (212 mg, 0.26 mmol) in 1,4-dioxane:H₂O = 3:1 (7 mL) was heated to 80 °C for 2 h in sealed tube. The resulting solution was cooled to rt, and 4N KOH solution (4 mL) and MeOH was added. The reaction mixture was then heated to 60 °C and stirred for 1 h (*N*-deprotection of benzenesulfonyl group). The mixture was diluted with water and neutralized with 6 N HCl solution in ice bath. The two-phase mixture was extracted with CH₂Cl₂. The combined organic layer was dried (MgSO₄) and concentrated in vacuo. The residue was purified with flash column chromatography (EtOAc/hexanes, gradient 1:2 to 1:1) to give the product as yellow solid (369 mg, 85%). ¹H NMR (400 MHz, chloroform-*d*) δ 9.41 (s, 1H), 8.38 (d, *J* = 2.0 Hz, 1H), 8.28 (d, *J* = 2.0 Hz, 1H), 7.44 (s, 1H),

7.13 (dd, *J* = 8.2, 2.0 Hz, 1H), 7.05 (d, *J* = 2.0 Hz, 1H), 6.97 (d, *J* = 8.2 Hz, 1H), 3.95 (s, 3H), 3.92 (s, 3H).

3-(3,4-Dimethoxyphenyl)-5-(4,4,5,5-tetramethyl-1,3,2-dioxaborolan-2-yl)-1H-pyrrolo[2,3-*b*]pyridine (**47**). A solution of 5-bromo-3-(3,4-dimethoxyphenyl)-1H-pyrrolo[2,3-*b*]pyridine (75 mg, 0.23 mmol), bis(pinacolato)diboron (74.6 mg, 0.29 mmol), KOAc (44.4 mg, 0.452 mmol), and PdCl₂(dppf)·CH₂Cl₂ (37 mg, 0.045 mmol) in anhydrous 1,4-dioxane was heated to 90 °C for 12 h under an atmosphere of N₂. The reaction mixture was cooled to rt and concentrated in vacuo. The residue was diluted with CH₂Cl₂ and MeOH and then filtered through a short pad of silica (SiO₂) and Celite eluting with CH₂Cl₂ and MeOH (15:1). The filtrate was concentrated in vacuo then purified by flash column chromatography (EtOAc/hexanes, gradient 1:3 to 1:1) to give **47** as brown solid (63.9 mg, 74%). ¹H NMR (300 MHz, chloroform-*d*) δ 12.14 (s, 1H), 8.82 (d, *J* = 1.4 Hz, 1H), 8.68 (d, *J* = 1.4 Hz, 1H), 7.54 (s, 1H), 7.28 (dd, *J* = 8.3, 2.0 Hz, 1H), 7.17 (d, *J* = 2.0 Hz, 1H), 7.02 (d, *J* = 8.3 Hz, 1H), 3.99 (s, 3H), 3.96 (s, 3H), 1.41 (s, 12H).

General Procedure (GP II) for Suzuki Coupling. 3-(3-(3,4-Dimethoxyphenyl)-1H-pyrrolo[2,3-*b*]pyridin-5-yl)aniline (**4**). A solution of 5-bromo-3-(3,4-dimethoxyphenyl)-1H-pyrrolo[2,3-*b*]pyridine (40 mg, 0.12 mmol), 3-aminophenylboronic acid (23 mg, 0.15 mmol), Cs₂CO₃ (78 mg, 0.24 mmol), and PdCl₂(dppf)·CH₂Cl₂ (20 mg, 0.024

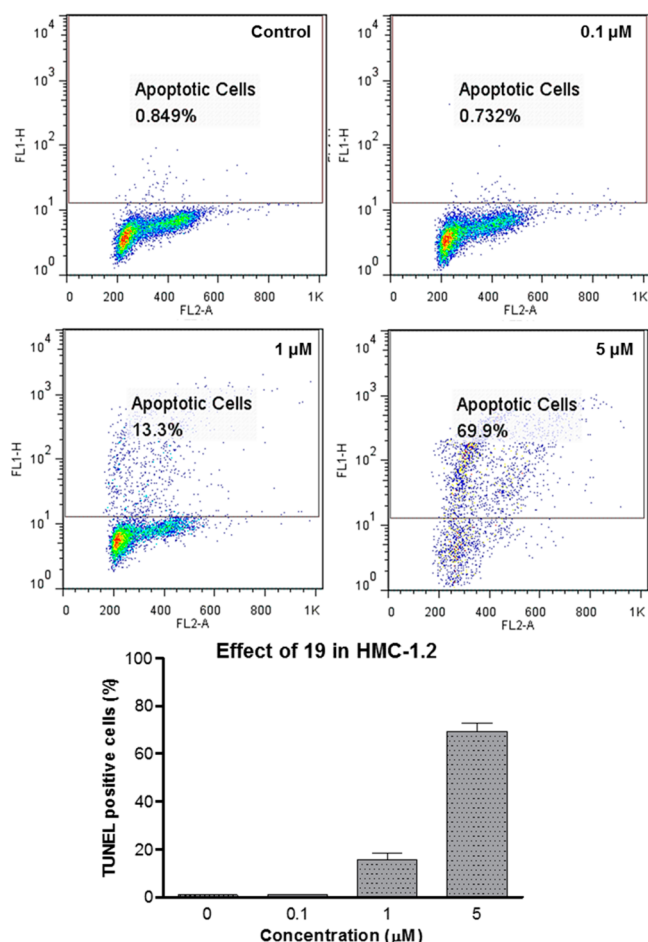


Figure 10. Effect of **19** on apoptosis in HMC-1.2 cells. HMC-1.2 cells were treated with various concentrations of **19** for 48 h, and apoptosis was determined by flow cytometry using TUNEL staining.

mmol) in 1,4-dioxane/H₂O = 3:1 (1 mL) was charged in capped tube and was heated to 100 °C for 3 h. The reaction mixture was cooled to room temperature and concentrated in vacuo. The residue was diluted with CH₂Cl₂, and organic phase was extracted with CH₂Cl₂. The combined organic layer was dried with MgSO₄ and concentrated in vacuo. The mixture was purified with flash column chromatography (CH₂Cl₂/MeOH, gradient 30:1 to 15:1) to give the product as white

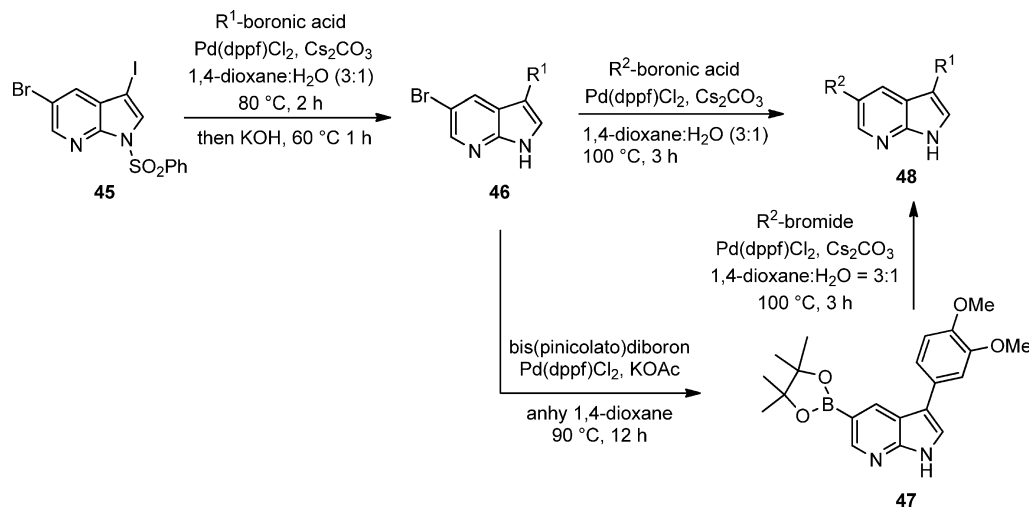
solid (11 mg, 27%). ¹H NMR (400 MHz, chloroform-*d*) δ 10.57 (s, 1H), 8.56 (d, *J* = 2.0 Hz, 1H), 8.32 (d, *J* = 2.0 Hz, 1H), 7.48 (s, 1H), 7.25 (t, *J* = 7.8 Hz, 1H), 7.20 (dd, *J* = 8.3, 2.0 Hz, 1H), 7.13 (d, *J* = 2.0 Hz, 1H), 7.01 (d, *J* = 7.8 Hz, 1H), 6.97 (d, *J* = 8.3 Hz, 1H), 6.92 (s, 1H), 6.69 (d, *J* = 7.8 Hz, 1H), 3.93 (s, 3H), 3.92 (s, 3H), 3.00 (br, 2H). ¹³C NMR (150 MHz, chloroform-*d*) δ 149.4, 148.6, 147.9, 146.9, 142.5, 140.8, 130.3, 129.9, 127.8, 126.6, 122.2, 119.6, 118.6, 117.9, 116.7, 114.1, 113.9, 111.9, 110.9, 56.1. HRMS (EI+) *m/z* calcd for C₂₁H₁₉N₃O₂ [M + H]⁺, 346.1556; found, 346.1543.

N-(5-(3-(3,4-Dimethoxyphenyl)-1*H*-pyrrolo[2,3-*b*]pyridin-5-yl)-pyridin-3-yl)benzenesulfonamide (**1**). Benzenesulfonyl chloride (10.7 μL, 0.084 mmol), pyridine (11.3 μL, 0.14 mmol), and dichloromethane (1 mL) was added to 5-(3-(3,4-dimethoxyphenyl)-1*H*-pyrrolo[2,3-*b*]pyridin-5-yl)pyridin-3-amine (24.3 mg, 0.07 mmol). The reaction mixture was stirred at rt for overnight and then diluted with DCM and brine. Organic phase was extracted with DCM, dried over MgSO₄. The concentrated crude was purified with flash column chromatography (CH₂Cl₂/MeOH, gradient 30:1 to 20:1) to give **1** (11.1 mg, 33%). ¹H NMR (400 MHz, DMSO-*d*₆) δ 12.05 (s, 1H), 10.83 (s, 1H), 8.67 (d, *J* = 2.0 Hz, 1H), 8.44 (d, *J* = 2.0 Hz, 1H), 8.30 (s, 2H), 7.88–7.77 (m, 4H), 7.64–7.54 (m, 3H), 7.29–7.26 (m, 2H), 7.03 (d, *J* = 8.9 Hz, 1H), 3.85 (s, 3H), 3.79 (s, 3H). MS (EI+) *m/z* calcd for C₂₆H₂₂N₄O₄S [M + H]⁺, 487.1; found, 487.2.

5-(3-(3,4-Dimethoxyphenyl)-1*H*-pyrrolo[2,3-*b*]pyridin-5-yl)-pyridin-3-amine (**3**). Compound **3** was prepared (42.6 mg, 40%) according to GP II (CH₂Cl₂/MeOH, gradient 20:1 to 15:1) from 5-bromo-3-(3,4-dimethoxyphenyl)-1*H*-pyrrolo[2,3-*b*]pyridine (101 mg, 0.3 mmol) and 5-(4,4,5,5-tetramethyl-1,3,2-dioxaborolan-2-yl)pyridin-3-amine (81 mg, 0.368 mmol) as white solid. ¹H NMR (400 MHz, DMSO-*d*₆) δ 11.96 (s, 1H), 8.49 (s, 1H), 8.33 (s, 1H), 8.12 (s, 1H), 7.94 (s, 1H), 7.86 (s, 1H), 7.29 (d, *J* = 8.2 Hz, 1H), 7.23–7.30 (m, 2H), 7.02 (d, *J* = 8.2 Hz, 1H), 5.42 (s, 2H), 3.84 (s, 3H), 3.78 (s, 3H). ¹³C NMR (100 MHz, DMSO-*d*₆) δ 149.2, 148.7, 147.3, 144.9, 141.5, 135.4, 135.1, 134.6, 127.7, 126.3, 125.3, 124.1, 118.7, 117.9, 117.4, 114.8, 112.4, 110.7, 55.6. HRMS (EI+) *m/z* calcd for C₂₀H₁₈N₄O₂ [M + H]⁺, 347.1508; found, 347.1508.

3-(3-(3,4-Dimethoxyphenyl)-1*H*-pyrrolo[2,3-*b*]pyridin-5-yl)-benzotrile (**5**). Compound **5** was prepared (31.5 mg, 59%) according to GP II (EtOAc/hexanes, gradient 1:1) from 5-bromo-3-(3,4-dimethoxyphenyl)-1*H*-pyrrolo[2,3-*b*]pyridine (50 mg, 0.15 mmol) and (3-cyanophenyl)boronic acid (26.4 mg, 0.18 mmol) as white solid. ¹H NMR (400 MHz, DMSO-*d*₆) δ 11.98 (s, 1H), 8.61 (d, *J* = 2.1 Hz, 1H), 8.49 (d, *J* = 2.1 Hz, 1H), 8.30 (s, 1H), 8.12 (d, *J* = 7.8 Hz, 1H), 7.86 (s, 1H), 7.81 (d, *J* = 7.8 Hz, 1H), 7.67 (t, *J* = 7.8 Hz, 1H), 7.35 (dd, *J* = 8.2, 2.0 Hz, 1H), 7.27 (d, *J* = 2.0 Hz, 1H), 7.03 (d, *J* = 8.3 Hz, 1H), 3.85 (s, 3H), 3.78 (s, 3H). ¹³C NMR (100 MHz, DMSO-*d*₆) δ 149.2, 148.8, 147.3, 141.9, 140.3, 131.8, 130.6, 130.4,

Scheme 1. Synthesis of 7-Azaindole Derivatives



130.1, 127.6, 126.5, 125.9, 124.2, 118.9, 118.8, 117.4, 115.1, 112.4, 112.1, 110.7, 55.6. HRMS (EI+) m/z calcd for $C_{22}H_{17}N_3O_2$ [$M + Na$]⁺, 378.1218; found, 378.1217.

3-(3-(3,4-Dimethoxyphenyl)-1H-pyrrolo[2,3-b]pyridin-5-yl)-N,N-dimethylaniline (6). Compound 6 was prepared (13.7 mg, 30%) according to GP II (EtOAc/hexanes, gradient 1:1) from 5-bromo-3-(3,4-dimethoxyphenyl)-1H-pyrrolo[2,3-b]pyridine (40 mg, 0.122 mmol) and (3-(dimethylamino)phenyl) boronic acid (24.2 mg, 0.146 mmol) as white solid. ¹H NMR (400 MHz, DMSO-*d*₆) δ 11.85 (s, 1H), 8.51 (d, *J* = 2.1 Hz, 1H), 8.33 (d, *J* = 2.1 Hz, 1H), 7.81 (s, 1H), 7.29–7.21 (m, 3H), 7.03 (d, *J* = 7.5 Hz, 1H), 6.99–6.94 (m, 2H), 6.72 (d, *J* = 7.5 Hz, 1H), 3.84 (s, 3H), 3.77 (s, 3H), 2.95 (s, 6H). ¹³C NMR (100 MHz, DMSO-*d*₆) δ 150.9, 149.1, 148.5, 147.2, 142.0, 139.9, 129.6, 129.4, 127.9, 125.3, 123.8, 118.5, 117.3, 115.2, 114.7, 112.5, 111.1, 111.0, 110.6, 55.6, 55.5, 40.2. HRMS (EI+) m/z calcd for $C_{23}H_{23}N_3O_2$ [$M + H$]⁺, 374.1869; found, 374.1845.

3-(3-(3,4-Dimethoxyphenyl)-5-(*m*-tolyl)-1H-pyrrolo[2,3-b]pyridine (7). Compound 7 was prepared (9.9 mg, 60%) according to GP II (CH₂Cl₂/MeOH, gradient 60:1 to 30:1) from 5-bromo-3-(3,4-dimethoxyphenyl)-1H-pyrrolo[2,3-b]pyridine (16 mg, 0.048 mmol) and *m*-tolylboronic acid (7.8 mg, 0.58 mmol) as white solid. ¹H NMR (400 MHz, DMSO-*d*₆) δ 11.87 (s, 1H), 8.52 (d, *J* = 2.1 Hz, 1H), 8.34 (d, *J* = 2.1 Hz, 1H), 7.81 (s, 1H), 7.54 (s, 1H), 7.51 (d, *J* = 7.6 Hz, 1H), 7.36 (t, *J* = 7.6 Hz, 1H), 7.29 (dd, *J* = 8.2, 2.1 Hz, 1H), 7.25 (d, *J* = 2.1 Hz, 1H), 7.17 (d, *J* = 7.6 Hz, 1H), 7.03 (d, *J* = 8.2 Hz, 1H), 3.84 (s, 3H), 3.77 (s, 3H), 2.38 (s, 3H). ¹³C NMR (100 MHz, DMSO-*d*₆) δ 149.2, 148.5, 147.3, 141.8, 139.0, 138.1, 128.8, 128.7, 127.8, 127.7, 127.5, 125.2, 124.1, 123.9, 118.7, 117.4, 114.8, 112.5, 110.7, 55.6, 55.6, 21.1. HRMS (EI+) m/z calcd for $C_{22}H_{20}N_3O_2$ [$M + Na$]⁺, 367.1422; found, 367.1423.

3-(3-(3,4-Dimethoxyphenyl)-5-(3-fluorophenyl)-1H-pyrrolo[2,3-b]pyridine (8). Compound 8 was prepared (18.2 mg, 65%) according to GP II (EA/HX, gradient 1:3 to 1:1) from 5-bromo-3-(3,4-dimethoxyphenyl)-1H-pyrrolo[2,3-b]pyridine (26.5 mg, 0.08 mmol) and 3-fluorophenylboronic acid (15.7 mg, 0.1 mmol). ¹H NMR (400 MHz, chloroform-*d*) δ 10.80 (s, 1H), 8.59 (s, 1H), 8.34 (s, 1H), 7.53 (s, 1H), 7.45–7.39 (m, 2H), 7.31–7.33 (m, 1H), 7.21 (dd, *J* = 8.2, 2.0 Hz, 1H), 7.13 (d, *J* = 2.0 Hz, 1H), 7.04–7.08 (m, 1H), 6.99 (d, *J* = 8.2 Hz, 1H), 3.94 (s, 3H), 3.93 (s, 3H). MS (EI+) m/z calcd for $C_{21}H_{17}FN_3O_2$ [$M + H$]⁺, 349.1; found, 349.2.

3-(3-(3,4-Dimethoxyphenyl)-5-phenyl-1H-pyrrolo[2,3-b]pyridine (9). Compound 9 was prepared (42.4 mg, 43%) according to GP II (EtOAc/CH₂Cl₂, gradient 1:5 to 1:3) from 5-bromo-3-(3,4-dimethoxyphenyl)-1H-pyrrolo[2,3-b]pyridine (99 mg, 0.3 mmol) and phenylboronic acid (43.9 mg, 0.36 mmol) as white solid. ¹H NMR (400 MHz, chloroform-*d*) δ 11.19 (s, 1H), 8.62 (d, *J* = 2.1 Hz, 1H), 8.37 (d, *J* = 2.1 Hz, 1H), 7.67–7.61 (m, 2H), 7.53 (s, 1H), 7.48 (t, *J* = 7.5 Hz, 2H), 7.37 (t, *J* = 7.5 Hz, 1H), 7.22 (dd, *J* = 8.2, 2.0 Hz, 1H), 7.15 (d, *J* = 2.0 Hz, 1H), 6.98 (d, *J* = 8.2 Hz, 1H), 3.94 (s, 3H), 3.93 (s, 3H). ¹³C NMR (100 MHz, DMSO-*d*₆) δ 149.27, 148.6, 147.3, 141.8, 139.1, 129.0, 128.6, 127.8, 127.1, 126.9, 125.3, 124.0, 118.7, 117.4, 114.9, 112.5, 110.6, 55.6. HRMS (EI+) m/z calcd for $C_{21}H_{18}N_3O_2$ [$M + Na$]⁺, 353.1266; found, 353.1253.

3-(3-(3,4-Dimethoxyphenyl)-5-(pyridin-4-yl)-1H-pyrrolo[2,3-b]pyridine (10). Compound 10 was prepared (19.9 mg, 72%) according to GP II (CH₂Cl₂/MeOH, gradient 30:1 to 10:1) from 5-bromo-3-(3,4-dimethoxyphenyl)-1H-pyrrolo[2,3-b]pyridine (28 mg, 0.084 mmol) and 4-pyridinylboronic acid (12.4 mg, 0.101 mmol) as white solid. ¹H NMR (400 MHz, chloroform-*d*) δ 10.01 (s, 1H), 8.72–8.65 (m, 3H), 8.40 (d, *J* = 2.0 Hz, 1H), 7.56–7.58 (m, 2H), 7.52 (s, 1H), 7.20 (dd, *J* = 8.3, 2.0 Hz, 1H), 7.12 (d, *J* = 2.0 Hz, 1H), 7.00 (d, *J* = 8.3 Hz, 1H), 3.95 (s, 3H), 3.94 (s, 3H). ¹³C NMR (100 MHz, DMSO-*d*₆) δ 150.1, 149.3, 149.2, 147.4, 146.1, 141.8, 127.5, 125.7, 125.4, 124.4, 121.4, 118.8, 117.4, 115.2, 112.5, 110.7, 55.6. HRMS (EI+) m/z calcd for $C_{20}H_{17}N_3O_2$ [$M + H$]⁺, 332.1399; found, 332.1372.

3-(3-(3,4-Dimethoxyphenyl)-5-(pyridin-3-yl)-1H-pyrrolo[2,3-b]pyridine (11). Compound 11 was prepared (31 mg, 62%) according to GP II (CH₂Cl₂/MeOH, gradient 30:1 to 15:1) from 5-bromo-3-(3,4-dimethoxyphenyl)-1H-pyrrolo[2,3-b]pyridine (50 mg, 0.15 mmol) and 3-pyridinylboronic acid (22.1 mg, 0.18 mmol) as white solid. ¹H NMR

(400 MHz, DMSO-*d*₆) δ 12.00 (s, 1H), 8.99 (s, 1H), 8.60 (d, *J* = 2.2 Hz, 1H), 8.56–8.57 (m, 1H), 8.47 (d, *J* = 2.2 Hz, 1H), 8.17 (d, *J* = 8.0 Hz, 1H), 7.87 (s, 1H), 7.48 (dd, *J* = 8.0, 4.8 Hz, 1H), 7.33 (dd, *J* = 8.2, 2.1 Hz, 1H), 7.29 (d, *J* = 2.1 Hz, 1H), 7.02 (d, *J* = 8.2 Hz, 1H), 3.85 (s, 3H), 3.78 (s, 3H). ¹³C NMR (100 MHz, DMSO-*d*₆) δ 149.2, 148.8, 147.9, 147.3, 141.8, 134.7, 134.5, 127.6, 125.8, 125.5, 124.2, 123.9, 118.8, 117.5, 115.0, 112.4, 110.7, 55.6, 55.6. HRMS (EI+) m/z calcd for $C_{20}H_{17}N_3O_2$ [$M + H$]⁺, 332.1399; found, 332.1385.

3-(3-(3,4-Dimethoxyphenyl)-5-*o*-tolyl-1H-pyrrolo[2,3-b]pyridine (12). Compound 12 was prepared (13.3 mg, 68%) according to GP II (CH₂Cl₂/MeOH, gradient 30:1 to 10:1) from 5-bromo-3-(3,4-dimethoxyphenyl)-1H-pyrrolo[2,3-b]pyridine (18.9 mg, 0.057 mmol) and *o*-tolylboronic acid (9.3 mg, 0.068 mmol). ¹H NMR (400 MHz, DMSO-*d*₆) δ 11.90 (s, 1H), 8.22 (d, *J* = 2.1 Hz, 1H), 8.12 (d, *J* = 2.1 Hz, 1H), 7.84 (s, 1H), 7.27–7.32 (m, 4H), 7.25–7.22 (m, 2H), 6.99 (d, *J* = 8.7 Hz, 1H), 3.82 (s, 3H), 3.76 (s, 3H), 2.28 (s, 3H). MS (EI+) m/z calcd for $C_{22}H_{20}N_3O_2$ [$M + H$]⁺, 345.2; found, 345.2.

2-(3-(3,4-Dimethoxyphenyl)-1H-pyrrolo[2,3-b]pyridin-5-yl)aniline (13). Compound 13 was prepared (14.7 mg, 67%) according to GP II (CH₂Cl₂/MeOH, gradient 30:1 to 1:1) from 5-bromo-3-(3,4-dimethoxyphenyl)-1H-pyrrolo[2,3-b]pyridine (21.4 mg, 0.064 mmol) and 2-aminophenylboronic acid (10.5 mg, 0.0768 mmol). ¹H NMR (400 MHz, chloroform-*d*) δ 10.21 (s, 1H), 8.44 (d, *J* = 2.0 Hz, 1H), 8.30 (d, *J* = 2.0 Hz, 1H), 7.52 (s, 1H), 7.21–7.17 (m, 3H), 7.13 (d, *J* = 2.0 Hz, 1H), 6.94 (d, *J* = 8.2 Hz, 1H), 6.86 (d, *J* = 7.7 Hz, 1H), 6.80 (d, *J* = 7.7 Hz, 1H), 3.93 (s, 3H), 3.91 (s, 3H), 3.75 (s, 2H). MS (EI+) m/z calcd for $C_{21}H_{19}N_3O_2$ [$M + H$]⁺, 346.2; found, 346.2.

4-(3-(3,4-Dimethoxyphenyl)-1H-pyrrolo[2,3-b]pyridin-5-yl)benzotrile (14). Compound 14 was prepared (15.1 mg, 48%) according to GP III (EtOAc/hexanes, gradient 1:1 to 2:1) from 3-(3,4-dimethoxyphenyl)-5-(4,4,5,5-tetramethyl-1,3,2-dioxaborolan-2-yl)-1H-pyrrolo[2,3-b]pyridine (34 mg, 0.0894 mmol) and 4-bromobenzotrile (19.5 mg, 0.107 mmol). ¹H NMR (400 MHz, chloroform-*d*) δ 10.61 (s, 1H), 8.60 (d, *J* = 2.0 Hz, 1H), 8.35 (d, *J* = 2.0 Hz, 1H), 7.76–7.71 (m, 4H), 7.54 (s, 1H), 7.20 (dd, *J* = 8.2, 1.9 Hz, 1H), 7.12 (d, *J* = 1.9 Hz, 1H), 6.99 (d, *J* = 8.2 Hz, 1H), 3.94 (s, 3H), 3.93 (s, 3H). MS (EI+) m/z calcd for $C_{22}H_{17}N_3O_2$ [$M + H$]⁺, 356.2; found, 356.2.

3-(3-(3,4-Dimethoxyphenyl)-5-(4-fluorophenyl)-1H-pyrrolo[2,3-b]pyridine (15). Compound 15 was prepared (8.4 mg, 31%) according to GP II (CH₂Cl₂/MeOH, gradient 30:1 to 10:1) from 5-bromo-3-(3,4-dimethoxyphenyl)-1H-pyrrolo[2,3-b]pyridine (26 mg, 0.078 mmol) and 4-fluorophenylboronic acid (13.2 mg, 0.094 mmol). ¹H NMR (400 MHz, DMSO-*d*₆) δ 11.90 (s, 1H), 8.52 (d, *J* = 2.1 Hz, 1H), 8.35 (d, *J* = 2.1 Hz, 1H), 7.83 (s, 1H), 7.77–7.83 (m, 2H), 7.32–7.28 (m, 3H), 7.26 (d, *J* = 2.0 Hz, 1H), 7.03 (d, *J* = 8.2 Hz, 1H), 3.84 (s, 3H), 3.78 (s, 3H). MS (EI+) m/z calcd for $C_{21}H_{17}FN_3O_2$ [$M + H$]⁺, 349.1; found, 349.1.

5-(4-Chlorophenyl)-3-(3,4-dimethoxyphenyl)-1H-pyrrolo[2,3-b]pyridine (16). Compound 16 was prepared (20.3 mg, 76%) according to GP II (EtOAc/hexanes, gradient 1:3 to 1:1) from 5-bromo-3-(3,4-dimethoxyphenyl)-1H-pyrrolo[2,3-b]pyridine (24.3 mg, 0.0735 mmol) and 4-chlorophenylboronic acid (13.8 mg, 0.088 mmol). ¹H NMR (400 MHz, chloroform-*d*) δ 9.39 (s, 1H), 8.54 (d, *J* = 2.1 Hz, 1H), 8.29 (d, *J* = 2.1 Hz, 1H), 7.55 (d, *J* = 8.5 Hz, 2H), 7.47 (s, 1H), 7.43 (d, *J* = 8.5 Hz, 2H), 7.20 (dd, *J* = 8.2, 2.0 Hz, 1H), 7.12 (d, *J* = 2.0 Hz, 1H), 6.98 (d, *J* = 8.2 Hz, 1H), 3.94 (s, 3H), 3.93 (s, 3H). MS (EI+) m/z calcd for $C_{21}H_{17}ClN_3O_2$ [$M + H$]⁺, 365.1; found, 365.1.

3-(3-(3,4-Dimethoxyphenyl)-5-*p*-tolyl-1H-pyrrolo[2,3-b]pyridine (17). Compound 17 was prepared (34.4 mg, 57%) according to GP II (CH₂Cl₂/MeOH, gradient 30:1 to 15:1) from 5-bromo-3-(3,4-dimethoxyphenyl)-1H-pyrrolo[2,3-b]pyridine (58 mg, 0.174 mmol) and *p*-tolylboronic acid (28.5 mg, 0.209 mmol). ¹H NMR (400 MHz, chloroform-*d*) δ 11.34 (s, 1H), 8.60 (d, *J* = 2.1 Hz, 1H), 8.35 (d, *J* = 2.1 Hz, 1H), 7.51–7.54 (m, 3H), 7.28 (d, *J* = 7.7 Hz, 2H), 7.21 (dd, *J* = 8.2, 2.0 Hz, 1H), 7.15 (d, *J* = 2.0 Hz, 1H), 6.97 (d, *J* = 8.2 Hz, 1H), 3.93 (s, 6H), 2.41 (s, 3H). MS (EI+) m/z calcd for $C_{22}H_{20}N_3O_2$ [$M + H$]⁺, 345.2; found, 345.2.

3-(3-(3,4-Dimethoxyphenyl)-5-(4-methoxyphenyl)-1H-pyrrolo[2,3-b]pyridine (18). Compound 18 was prepared (22.2 mg, 68%) according to GP II (EtOAc/hexanes, gradient 1:3 to 1:1) from 5-

bromo-3-(3,4-dimethoxyphenyl)-1*H*-pyrrolo[2,3-*b*]pyridine (29.9 mg, 0.09 mmol) and 4-methoxyphenylboronic acid (16.4 mg, 0.108 mmol). ¹H NMR (400 MHz, chloroform-*d*) δ 9.94 (s, 1H), 8.55 (d, *J* = 2.1 Hz, 1H), 8.30 (d, *J* = 2.1 Hz, 1H), 7.55 (d, *J* = 8.7 Hz, 2H), 7.48 (s, 1H), 7.21 (dd, *J* = 8.2, 2.0 Hz, 1H), 7.15 (d, *J* = 2.0 Hz, 1H), 7.01 (d, *J* = 8.7 Hz, 2H), 6.98 (d, *J* = 8.2 Hz, 1H), 3.94 (s, 3H), 3.93 (s, 3H), 3.85 (s, 3H). MS (EI+) *m/z* calcd for C₂₂H₂₀N₂O₃ [M + H]⁺, 361.2; found, 361.2.

3,5-Bis(3,4-dimethoxyphenyl)-1*H*-pyrrolo[2,3-*b*]pyridine (19). Compound **19** was prepared (27 mg, 58%) according to GP II (EtOAc/hexanes, 2:1) from 5-bromo-3-(3,4-dimethoxyphenyl)-1*H*-pyrrolo[2,3-*b*]pyridine (40 mg, 0.12 mmol) and 3,4-dimethoxyphenylboronic acid (26.2 mg, 0.14 mmol) as white solid. ¹H NMR (400 MHz, DMSO-*d*₆) δ 11.86 (s, 1H), 8.54 (d, *J* = 2.1 Hz, 1H), 8.35 (d, *J* = 2.1 Hz, 1H), 7.81 (s, 1H), 7.31–7.28 (m, 3H), 7.24 (dd, *J* = 8.3, 2.1 Hz, 1H), 7.01–7.05 (m, 2H), 3.86 (s, 3H), 3.86 (s, 3H), 3.79 (s, 3H), 3.78 (s, 3H). ¹³C NMR (100 MHz, DMSO-*d*₆) δ 149.2, 149.2, 148.3, 148.2, 147.2, 141.8, 131.9, 128.7, 127.9, 125.0, 123.8, 119.1, 118.6, 117.3, 114.7, 112.5, 112.4, 111.0, 110.6, 55.6, 55.5. HRMS (EI+) *m/z* calcd for C₂₃H₂₂N₂O₄ [M + Na]⁺, 413.1477; found, 413.1482.

5-(3,5-Difluorophenyl)-3-(3,4-dimethoxyphenyl)-1*H*-pyrrolo[2,3-*b*]pyridine (20). Compound **20** was prepared (24.1 mg, 82%) according to GP II (EtOAc/hexanes, gradient 1:3 to 1:1) from 5-bromo-3-(3,4-dimethoxyphenyl)-1*H*-pyrrolo[2,3-*b*]pyridine (26.8 mg, 0.0804 mmol) and 3,5-difluorophenylboronic acid (15.2 mg, 0.0965 mmol). ¹H NMR (400 MHz, chloroform-*d*) δ 10.23 (s, 1H), 8.48 (d, *J* = 2.0 Hz, 1H), 8.30 (d, *J* = 2.0 Hz, 1H), 7.51 (s, 1H), 7.45 (td, *J* = 8.6, 6.4 Hz, 1H), 7.19 (dd, *J* = 8.1, 2.0 Hz, 1H), 7.14 (d, *J* = 2.0 Hz, 1H), 7.01–6.92 (m, 3H), 3.94 (s, 3H), 3.92 (s, 3H). MS (EI+) *m/z* calcd for C₂₁H₁₆F₂N₂O₂ [M + H]⁺, 367.1; found, 367.1.

3-(3-(3,4,5-Trimethoxyphenyl)-1*H*-pyrrolo[2,3-*b*]pyridin-5-yl)-aniline (21). 5-Bromo-3-(3,4,5-trimethoxyphenyl)-1*H*-pyrrolo[2,3-*b*]pyridine was prepared (91 mg, 77%) according to GP I from 5-bromo-3-iodo-1-(phenyl-sulfonyl)-1*H*-pyrrolo[2,3-*b*]pyridine (150 mg, 0.325 mmol) and (3,4,5-trimethoxyphenyl)boronic acid (82.6 mg, 0.390 mmol). ¹H NMR (400 MHz, chloroform-*d*) δ 9.62 (s, 1H), 8.39 (s, 1H), 8.27 (s, 1H), 7.46 (s, 1H), 6.75 (s, 2H), 3.93 (s, 6H), 3.89 (s, 3H). Compound **21** was prepared (42.3 mg, 47%) according to GP II (EA/HX 2:1) 5-bromo-3-(3,4,5-trimethoxyphenyl)-1*H*-pyrrolo[2,3-*b*]pyridine (87 mg, 0.24 mmol) and 3-aminophenylboronic acid (44.5 mg, 0.29 mmol) as white solid. ¹H NMR (400 MHz, DMSO-*d*₆) δ 11.92 (s, 1H), 8.47 (d, *J* = 2.0 Hz, 1H), 8.29 (d, *J* = 2.0 Hz, 1H), 7.86 (s, 1H), 7.12 (t, *J* = 7.8 Hz, 1H), 6.95 (s, 2H), 6.91 (s, 1H), 6.87 (d, *J* = 7.8 Hz, 1H), 6.56 (d, *J* = 7.8 Hz, 1H), 5.18 (s, 2H), 3.87 (s, 6H), 3.69 (s, 3H). ¹³C NMR (100 MHz, DMSO-*d*₆) δ 153.3, 149.2, 148.4, 141.7, 139.6, 135.9, 130.7, 129.5, 129.4, 124.7, 124.4, 117.3, 114.9, 114.5, 112.7, 112.4, 104.1, 60.15, 56.0. HRMS (EI+) *m/z* calcd for C₂₂H₂₁N₃O₃ [M + Na]⁺, 398.1481; found, 398.1471.

3-(3-(3-Fluoro-4-methoxyphenyl)-1*H*-pyrrolo[2,3-*b*]pyridin-5-yl)-aniline (22). 5-Bromo-3-(3-fluoro-4-methoxyphenyl)-1*H*-pyrrolo[2,3-*b*]pyridine was prepared (85.1 mg, 61%) according to GP I from 5-bromo-3-iodo-1-(phenyl-sulfonyl)-1*H*-pyrrolo[2,3-*b*]pyridine (200 mg, 0.432 mmol) and 3-fluoro-4-methoxyphenylboronic acid (88.1 mg, 0.518 mmol). ¹H NMR (400 MHz, chloroform-*d*) δ 9.79 (s, 1H), 8.38 (d, *J* = 2.1 Hz, 1H), 8.28 (d, *J* = 2.1 Hz, 1H), 7.44 (s, 1H), 7.32–7.28 (m, 1H), 7.28–7.26 (m, 1H), 7.04 (t, *J* = 8.8 Hz, 1H), 3.93 (s, 3H). Compound **22** was prepared (37 mg, 46.1%) according to GP II (EA/HX, gradient 2:1) from 5-bromo-3-(3-fluoro-4-methoxyphenyl)-1*H*-pyrrolo[2,3-*b*]pyridine (77.3 mg, 0.24 mmol) and 3-aminophenylboronic acid (44.8 mg, 0.29 mmol) as white solid. ¹H NMR (400 MHz, DMSO-*d*₆) δ 11.93 (s, 1H), 8.47 (d, *J* = 2.1 Hz, 1H), 8.28 (d, *J* = 2.1 Hz, 1H), 7.86 (s, 1H), 7.52–7.60 (m, 2H), 7.23 (t, *J* = 8.9 Hz, 1H), 7.12 (t, *J* = 7.8 Hz, 1H), 6.91 (s, 1H), 6.87 (d, *J* = 7.8 Hz, 1H), 6.57 (d, *J* = 7.8 Hz, 1H), 5.15 (s, 2H), 3.86 (s, 3H). ¹³C NMR (100 MHz, DMSO-*d*₆) δ 151.9 (d, *J* = 243.2 Hz), 149.2, 148.4, 145.2 (d, *J* = 10.7 Hz), 141.8, 139.6, 129.6, 129.5, 128.3 (d, *J* = 7.0 Hz), 124.8, 124.3, 122.4 (d, *J* = 3.3 Hz), 117.1, 114.8, 114.4 (d, *J* = 2.3 Hz), 113.8 (d, *J* = 18.4 Hz), 113.3 (d, *J* = 1.9 Hz), 112.8, 112.5, 56.1. HRMS (EI+) *m/z* calcd for C₂₀H₁₆FN₃O [M + H]⁺, 334.1356; found, 334.1326.

2,3'-(1*H*-Pyrrolo[2,3-*b*]pyridine-3,5-diyl)dianiline (23). 2-(5-Bromo-1*H*-pyrrolo[2,3-*b*]pyridin-3-yl)aniline was prepared (32.5 mg, 50%) according to GP I (EtOAc/hexanes, gradient 1:3 to 1:1) from 5-bromo-3-iodo-1-(phenylsulfonyl)-1*H*-pyrrolo[2,3-*b*]pyridine (105.2 mg, 0.2278 mmol) and 2-aminophenylboronic acid (37.4 mg, 0.2734 mmol). ¹H NMR (300 MHz, chloroform-*d*) 11.42 (s, 1H), 8.64 (d, *J* = 2.0 Hz, 1H), 8.45 (d, *J* = 2.0 Hz, 1H), 7.80 (s, 1H), 7.56–7.47 (m, 2H), 7.18–7.13 (m, 2H). Compound **23** was prepared (8.9 mg, 26.3%) according to GP II (CH₂Cl₂/MeOH, gradient 30:1 to 15:1) from 2-(5-bromo-1*H*-pyrrolo[2,3-*b*]pyridin-3-yl)aniline (32.5 mg, 0.1128 mmol) and 3-aminophenylboronic acid (18.5 mg, 0.135 mmol). ¹H NMR (400 MHz, chloroform-*d*) δ 9.52 (s, 1H), 8.58 (d, *J* = 2.1 Hz, 1H), 8.11 (d, *J* = 2.1 Hz, 1H), 7.47 (s, 1H), 7.29 (d, *J* = 7.5 Hz, 1H), 7.23–7.14 (m, 2H), 7.00 (d, *J* = 7.5 Hz, 1H), 6.91 (s, 1H), 6.87–6.77 (m, 2H), 6.66 (d, *J* = 7.5 Hz, 1H), 3.83 (s, 2H), 3.74 (s, 2H). MS (EI+) *m/z* calcd for C₁₉H₁₆N₄ [M + H]⁺, 301.1; found, 301.2.

5-Bromo-3-(*p*-tolyl)-1*H*-pyrrolo[2,3-*b*]pyridine (24). 5-Bromo-3-(*p*-tolyl)-1*H*-pyrrolo[2,3-*b*]pyridine was prepared (22.4 mg, 36%) according to GP I (EtOAc/hexanes, gradient 1:4 to 1:1) from 5-bromo-3-iodo-1-(phenylsulfonyl)-1*H*-pyrrolo[2,3-*b*]pyridine (100 mg, 0.2168 mmol) and *p*-tolylboronic acid (37.4 mg, 0.2734 mmol). ¹H NMR (300 MHz, chloroform-*d*) 9.34 (s, 1H), 8.33 (s, 1H), 8.27 (s, 1H), 7.44–7.41 (m, 3H), 7.26–7.23 (m, 2H). Compound **24** was prepared (10.2 mg, 45.2%) according to GP II (CH₂Cl₂/MeOH, gradient 20:1 to 15:1) from 5-bromo-3-(*p*-tolyl)-1*H*-pyrrolo[2,3-*b*]pyridine (22.4 mg, 0.078 mmol) and 3-aminophenylboronic acid (14.6 mg, 0.094 mmol). ¹H NMR (400 MHz, DMSO-*d*₆) δ 11.88 (s, 1H), 8.45 (d, *J* = 2.1 Hz, 1H), 8.27 (d, *J* = 2.1 Hz, 1H), 7.82 (s, 1H), 7.63 (d, *J* = 7.9 Hz, 2H), 7.26 (d, *J* = 7.9 Hz, 2H), 7.11 (t, *J* = 7.7 Hz, 1H), 6.89 (s, 1H), 6.85 (d, *J* = 7.7 Hz, 1H), 6.57–6.54 (m, 1H), 5.15 (s, 2H), 2.33 (s, 3H). MS (EI+) *m/z* calcd for C₂₀H₁₇N₃ [M + H]⁺, 300.2; found, 300.2.

3-(3-(4-Methoxyphenyl)-1*H*-pyrrolo[2,3-*b*]pyridin-5-yl)aniline (25). 5-Bromo-3-(4-methoxyphenyl)-1*H*-pyrrolo[2,3-*b*]pyridine was prepared (118 mg, 60%) according to GP I from 5-bromo-3-iodo-1-(phenyl-sulfonyl)-1*H*-pyrrolo[2,3-*b*]pyridine (300 mg, 0.649 mmol) and 4-methoxyphenylboronic acid (118.4 mg, 0.78 mmol). ¹H NMR (300 MHz, chloroform-*d*) δ 9.29 (s, 1H), 8.36 (dd, *J* = 2.1, 0.4 Hz, 1H), 8.28 (d, *J* = 2.1 Hz, 1H), 7.49 (d, *J* = 8.8 Hz, 2H), 7.41 (s, 1H), 7.00 (d, *J* = 8.8 Hz, 2H), 3.85 (s, 3H). Compound **25** was prepared (83.7 mg, 69%) according to GP II (EtOAc/hexanes, 2:1) from 5-bromo-3-(4-methoxyphenyl)-1*H*-pyrrolo[2,3-*b*]pyridine (117 mg, 0.39 mmol) and 3-aminophenylboronic acid (71.8 mg, 0.46 mmol) as white solid. ¹H NMR (400 MHz, DMSO-*d*₆) δ 11.84 (s, 1H), 8.45 (d, *J* = 2.0 Hz, 1H), 8.26 (d, *J* = 2.0 Hz, 1H), 7.76 (s, 1H), 7.66 (d, *J* = 8.7 Hz, 2H), 7.12 (t, *J* = 7.7 Hz, 1H), 7.02 (d, *J* = 8.7 Hz, 2H), 6.90 (s, 1H), 6.85 (d, *J* = 7.7 Hz, 1H), 6.57 (d, *J* = 7.7 Hz, 1H), 5.15 (s, 2H), 3.78 (s, 3H). ¹³C NMR (100 MHz, DMSO-*d*₆) δ 157.5, 149.1, 148.4, 141.6, 139.6, 129.4, 129.4, 127.6, 127.4, 124.8, 123.5, 117.3, 114.7, 114.4, 112.7, 112.4, 55.1. HRMS (EI+) *m/z* calcd for C₂₀H₁₇N₃O [M + H]⁺, 316.1450; found, 316.1424.

3-(3-(3-Methoxyphenyl)-1*H*-pyrrolo[2,3-*b*]pyridin-5-yl)aniline (26). 5-Bromo-3-(3-methoxyphenyl)-1*H*-pyrrolo[2,3-*b*]pyridine was prepared (34.1 mg, 52%) according to GP I (EtOAc/hexanes, gradient 1:5 to 1:1) from 5-bromo-3-iodo-1-(phenylsulfonyl)-1*H*-pyrrolo[2,3-*b*]pyridine (99.7 mg, 0.216 mmol) and 3-methoxyphenylboronic acid (39.4 mg, 0.259 mmol). ¹H NMR (400 MHz, chloroform-*d*) δ 12.18 (s, 1H), 8.39 (d, *J* = 2.1 Hz, 1H), 8.32 (d, *J* = 2.1 Hz, 1H), 7.97 (s, 1H), 7.35 (t, *J* = 7.9 Hz, 1H), 7.28 (d, *J* = 7.9 Hz, 1H), 7.20 (s, 1H), 6.84 (d, *J* = 7.9 Hz, 1H). Compound **26** was prepared (6.5 mg, 36.8%) according to GP II (EtOAc/hexanes, gradient 1:1 to 2:1) from 5-bromo-3-(3-methoxyphenyl)-1*H*-pyrrolo[2,3-*b*]pyridine (17 mg, 0.056 mmol) and 3-aminophenylboronic acid (9.2 mg, 0.0672 mmol). ¹H NMR (300 MHz, chloroform-*d*) δ 10.63 (s, 1H), 8.58 (s, 1H), 8.37 (s, 1H), 7.56 (s, 1H), 7.38 (s, 1H), 7.27–7.20 (m, 3H), 7.03 (d, *J* = 8.1 Hz, 1H), 6.93 (s, 1H), 6.86 (d, *J* = 8.4 Hz, 1H), 6.70 (d, *J* = 8.4 Hz, 1H), 3.86 (s, 3H), 3.79 (s, 2H). MS (EI+) *m/z* calcd for C₂₀H₁₇N₃O [M + H]⁺, 316.1; found, 316.2.

3-(3-(3,5-Dimethoxyphenyl)-1H-pyrrolo[2,3-b]pyridin-5-yl)aniline (27). 5-Bromo-3-(3,5-dimethoxyphenyl)-1H-pyrrolo[2,3-b]pyridine was prepared (12.7 mg, 18%) according to GP I (EtOAc/hexanes, gradient 1:4 to 1:1) from 5-bromo-3-iodo-1-(phenylsulfonyl)-1H-pyrrolo[2,3-b]pyridine (100 mg, 0.216 mmol) and 3,5-dimethoxyphenylboronic acid (47.2 mg, 0.259 mmol). ¹H NMR (300 MHz, methanol-*d*₄) δ 8.31 (d, *J* = 2.1 Hz, 1H), 8.25 (d, *J* = 2.1 Hz, 1H), 7.61 (s, 1H), 7.16–7.14 (m, 2H), 7.02 (d, *J* = 8.9 Hz, 1H). Compound 27 was prepared (4.5 mg, 34%) according to GP II (EtOAc/hexanes, gradient 1:1 to 2:1) from 5-bromo-3-(3,5-dimethoxyphenyl)-1H-pyrrolo[2,3-b]pyridine (12.7 mg, 0.038 mmol) and 3-aminophenylboronic acid (6.2 mg, 0.0456 mmol). ¹H NMR (400 MHz, DMSO-*d*₆) δ 11.97 (s, 1H), 8.46 (d, *J* = 2.1 Hz, 1H), 8.25 (d, *J* = 2.1 Hz, 1H), 7.91 (s, 1H), 7.12 (t, *J* = 7.9 Hz, 1H), 6.89 (s, 1H), 6.85–6.83 (m, 3H), 6.56 (d, *J* = 7.9 Hz, 1H), 6.42 (s, 1H), 5.17 (s, 2H), 3.81 (s, 6H). MS (EI+) *m/z* calcd for C₂₁H₁₉N₃O₂ [M + H]⁺, 346.2; found, 346.2.

3,3'-(1H-Pyrrolo[2,3-b]pyridine-3,5-diyl)dianiline (28). 3-(5-Bromo-1H-pyrrolo[2,3-b]pyridin-3-yl)aniline was prepared (27.8 mg, 45%) according to GP I (EtOAc/hexanes, gradient 1:2 to 1:1) from 5-bromo-3-iodo-1-(phenylsulfonyl)-1H-pyrrolo[2,3-b]pyridine (100 mg, 0.216 mmol) and 3-aminophenylboronic acid (35.6 mg, 0.26 mmol). ¹H NMR (300 MHz, methanol-*d*₄) δ 8.35 (d, *J* = 2.1 Hz, 1H), 8.24 (d, *J* = 2.1 Hz, 1H), 7.57 (s, 1H), 7.16 (t, *J* = 7.9 Hz, 1H), 7.00 (s, 1H), 6.94–6.92 (m, 1H), 6.66 (dd, *J* = 7.9, 2.1 Hz, 1H). Compound 28 was prepared (6.8 mg, 23.5%) according to GP II (CH₂Cl₂/MeOH, gradient 30:1 to 15:1) from 3-(5-bromo-1H-pyrrolo[2,3-b]pyridin-3-yl)aniline (27.8 mg, 0.0965 mmol) and 3-aminophenylboronic acid (15.9 mg, 0.1158 mmol). ¹H NMR (400 MHz, DMSO-*d*₆) δ 11.83 (s, 1H), 8.43 (d, *J* = 2.1 Hz, 1H), 8.29 (d, *J* = 2.1 Hz, 1H), 7.71 (s, 1H), 7.12 (t, *J* = 7.8 Hz, 1H), 7.07 (t, *J* = 7.6 Hz, 1H), 6.97 (s, 1H), 6.88 (s, 1H), 6.86–6.83 (m, 2H), 6.56 (d, *J* = 7.8 Hz, 1H), 6.46 (d, *J* = 6.7 Hz, 1H), 5.15 (s, 2H), 5.10 (s, 2H). MS (EI+) *m/z* calcd for C₁₉H₁₆N₄ [M + H]⁺, 301.1; found, 301.2.

3-(3-(4-Chlorophenyl)-1H-pyrrolo[2,3-b]pyridin-5-yl)aniline (29). 5-Bromo-3-(4-chlorophenyl)-1H-pyrrolo[2,3-b]pyridine was prepared (19.2 mg, 28%) according to GP I (EtOAc/hexanes, gradient 1:3 to 1:1) from 5-bromo-3-iodo-1-(phenylsulfonyl)-1H-pyrrolo[2,3-b]pyridine (101.4 mg, 0.2195 mmol) and 4-chlorophenylboronic acid (41.2 mg, 0.2634 mmol). ¹H NMR (300 MHz, DMSO-*d*₆) δ 11.65 (s, 1H), 8.45 (d, *J* = 2.1 Hz, 1H), 8.33 (d, *J* = 2.1 Hz, 1H), 8.01 (s, 1H), 7.75 (d, *J* = 8.5 Hz, 2H), 7.46 (d, *J* = 8.5 Hz, 2H). Compound 29 was prepared (2.4 mg, 12%) according to GP II (CH₂Cl₂/MeOH, 30:1) from 5-bromo-3-(4-chlorophenyl)-1H-pyrrolo[2,3-b]pyridine (19.2 mg, 0.0624 mmol) and 3-aminophenylboronic acid (10.3 mg, 0.0749 mmol). ¹H NMR (400 MHz, DMSO-*d*₆) δ 12.02 (s, 1H), 8.46 (d, *J* = 2.1 Hz, 1H), 8.30 (d, *J* = 2.1 Hz, 1H), 7.94 (s, 1H), 7.79 (d, *J* = 8.5 Hz, 2H), 7.48 (d, *J* = 8.5 Hz, 2H), 7.12 (t, *J* = 7.8 Hz, 1H), 6.89 (s, 1H), 6.86 (d, *J* = 7.8 Hz, 1H), 6.57 (d, *J* = 7.8 Hz, 1H), 5.15 (s, 2H). MS (EI+) *m/z* calcd for C₁₉H₁₄ClN₃ [M + H]⁺, 320.1; found, 320.1.

N-(3-(3-(3,4-Dimethoxyphenyl)-1H-pyrrolo[2,3-b]pyridin-5-yl)phenyl)acetamide (30). Compound 30 was prepared (41.9 mg, 31%) according to GP II (CH₂Cl₂/MeOH, gradient 30:1 to 15:1) from 5-bromo-3-(3,4-dimethoxyphenyl)-1H-pyrrolo[2,3-b]pyridine (117 mg, 0.351 mmol) and *N*-(3-(4,4,5,5-tetramethyl-1,3,2-dioxaborolan-2-yl)phenyl)acetamide (110 mg, 0.421 mmol). ¹H NMR (400 MHz, DMSO-*d*₆) δ 11.91 (s, 1H), 10.02 (s, 1H), 8.50 (d, *J* = 2.0 Hz, 1H), 8.32 (d, *J* = 2.0 Hz, 1H), 7.91 (s, 1H), 7.84 (s, 1H), 7.59 (d, *J* = 7.1 Hz, 1H), 7.43–7.37 (m, 2H), 7.28–7.26 (m, 2H), 7.04 (d, *J* = 8.2 Hz, 1H), 3.85 (s, 3H), 3.78 (s, 3H), 2.06 (s, 3H). MS (EI+) *m/z* calcd for C₂₃H₂₁N₃O₃ [M + H]⁺, 388.2; found, 388.2.

(2-Amino-4-(3-(3,4-dimethoxyphenyl)-1H-pyrrolo[2,3-b]pyridin-5-yl)phenyl)(morpholino)methanone (31). Compound 31 was prepared (52.4 mg, 43%) according to GP II (CH₂Cl₂/MeOH, gradient 20:1 to 15:1) from 5-bromo-3-(3,4-dimethoxyphenyl)-1H-pyrrolo[2,3-b]pyridine (90 mg, 0.267 mmol) and (2-amino-4-(4,4,5,5-tetramethyl-1,3,2-dioxaborolan-2-yl)phenyl)(morpholino)methanone (107 mg, 0.321 mmol) as pale-yellow solid. ¹H NMR (400 MHz, DMSO-*d*₆) δ 11.90 (s, 1H), 8.51 (s, 1H), 8.33 (s, 1H), 7.82 (s, 1H), 7.28–7.25 (m, 2H), 7.12 (d, *J* = 7.8 Hz, 1H), 7.09 (s, 1H), 7.03 (d, *J* = 8.1 Hz, 1H), 6.96 (d, *J* = 7.8 Hz, 1H), 5.34 (s, 2H), 3.84 (s, 3H), 3.77

(s, 3H) 3.61–3.60 (m, 4H), 4H. ¹³C NMR (100 MHz, DMSO-*d*₆) δ 168.6, 149.2, 148.6, 147.3, 146.6, 141.6, 140.8, 128.8, 128.4, 127.8, 125.0, 124.0, 118.7, 117.6, 117.4, 114.9, 114.4, 113.8, 112.5, 110.7, 66.2, 55.6, 55.6. HRMS (EI+) *m/z* calcd for C₂₆H₂₆N₄O₄ [M + Na]⁺, 481.1852; found, 481.1866.

3-(3-(3,4-Dimethoxyphenyl)-5-(3,4,5-trimethoxyphenyl)-1H-pyrrolo[2,3-b]pyridine (32). Compound 32 was prepared (37 mg, 59%) according to GP II (EtOAc/hexanes, 2:1) from 5-bromo-3-(3,4-dimethoxyphenyl)-1H-pyrrolo[2,3-b]pyridine (50 mg, 0.15 mmol) and (3,4,5-trimethoxyphenyl) boronic acid (38.2 mg, 0.18 mmol) as white solid. ¹H NMR (400 MHz, DMSO-*d*₆) δ 11.89 (s, 1H), 8.57 (d, *J* = 2.1 Hz, 1H), 8.40 (d, *J* = 2.1 Hz, 1H), 7.82 (s, 1H), 7.32–7.29 (m, 2H), 7.02 (d, *J* = 8.1 Hz, 1H), 6.99 (s, 2H), 3.87 (s, 6H), 3.86 (s, 3H), 3.78 (s, 3H), 3.70 (s, 3H). ¹³C NMR (100 MHz, DMSO-*d*₆) δ 153.3, 149.2, 148.5, 147.2, 142.0, 136.8, 135.0, 128.9, 127.9, 125.5, 123.9, 118.6, 117.2, 114.8, 112.5, 110.6, 104.7, 60.0, 56.0, 55.6, 55.5. HRMS (EI+) *m/z* calcd for C₂₄H₂₄N₂O₅ [M + Na]⁺, 443.1583; found, 443.1566.

5-(3-(3,4-Dimethoxyphenyl)-1H-pyrrolo[2,3-b]pyridin-5-yl)-2-methylaniline (33). Compound 33 was prepared (31.8 mg, 57%) according to GP II (CH₂Cl₂/MeOH, gradient 60:1 to 30:1) from 5-bromo-3-(3,4-dimethoxyphenyl)-1H-pyrrolo[2,3-b]pyridine (50 mg, 0.15 mmol) and 2-methyl-5-(4,4,5,5-tetramethyl-1,3,2-dioxaborolan-2-yl)aniline (42 mg, 0.18 mmol) as white solid. ¹H NMR (400 MHz, DMSO-*d*₆) δ 11.82 (s, 1H), 8.44 (d, *J* = 2.1 Hz, 1H), 8.24 (d, *J* = 2.1 Hz, 1H), 7.79 (s, 1H), 7.26–7.23 (m, 2H), 7.04 (d, *J* = 8.0 Hz, 1H), 7.01 (d, *J* = 7.6 Hz, 1H), 6.95 (d, *J* = 1.9 Hz, 1H), 6.82 (dd, *J* = 7.6, 1.9 Hz, 1H), 4.91 (s, 2H), 3.84 (s, 3H), 3.78 (s, 3H), 2.08 (s, 3H). ¹³C NMR (100 MHz, DMSO-*d*₆) δ 149.2, 148.3, 147.2, 147.0, 141.6, 137.2, 130.5, 129.3, 127.9, 124.6, 123.7, 120.0, 118.5, 117.4, 114.7, 114.6, 112.5, 112.4, 110.6, 55.6, 55.6, 17.1. HRMS (EI+) *m/z* calcd for C₂₂H₂₁N₃O₂ [M + H]⁺, 360.1712; found, 360.1691.

5-(3-(3,4-Dimethoxyphenyl)-1H-pyrrolo[2,3-b]pyridin-5-yl)-2-methoxyaniline (34). Compound 34 was prepared (44.2 mg, 39%) according to GP II (CH₂Cl₂/MeOH, gradient 30:1) from 5-bromo-3-(3,4-dimethoxyphenyl)-1H-pyrrolo[2,3-b]pyridine (100 mg, 0.3 mmol) and 2-methoxy-5-(4,4,5,5-tetramethyl-1,3,2-dioxaborolan-2-yl)aniline (89.7 mg, 0.36 mmol) as white solid. ¹H NMR (400 MHz, chloroform-*d*) δ 10.98 (s, 1H), 8.52 (d, *J* = 2.0 Hz, 1H), 8.27 (d, *J* = 2.0 Hz, 1H), 7.46 (s, 1H), 7.19 (dd, *J* = 8.2, 2.0 Hz, 1H), 7.13 (d, *J* = 2.0 Hz, 1H), 6.97–6.95 (m, 3H), 6.87 (d, *J* = 8.7 Hz, 1H), 3.92 (s, 3H), 3.92 (s, 3H), 3.89 (s, 3H). ¹³C NMR (100 MHz, chloroform-*d*) δ 149.3, 148.3, 147.8, 146.8, 142.0, 136.6, 132.6, 130.1, 127.9, 126.3, 122.3, 119.6, 118.6, 117.4, 116.4, 114.0, 111.8, 110.8, 110.8, 56.0, 56.0, 55.6. HRMS (EI+) *m/z* calcd for C₂₂H₂₁N₃O₃ [M + H]⁺, 376.1661; found, 376.1635.

5-(Benzo[d][1,3]dioxol-5-yl)-3-(3,4-dimethoxyphenyl)-1H-pyrrolo[2,3-b]pyridine (35). Compound 35 was prepared (21.6 mg, 66%) according to GP II (EtOAc/hexanes, gradient 1:3 to 1:1) from 5-bromo-3-(3,4-dimethoxyphenyl)-1H-pyrrolo[2,3-b]pyridine (29 mg, 0.087 mmol) and 3,4-(methylenedioxy)phenyl boronic acid (17.3 mg, 0.1044 mmol). ¹H NMR (400 MHz, chloroform-*d*) δ 10.49 (s, 1H), 8.53 (d, *J* = 2.0 Hz, 1H), 8.27 (d, *J* = 2.0 Hz, 1H), 7.50 (s, 1H), 7.20 (dd, *J* = 8.2, 2.0 Hz, 1H), 7.14 (d, *J* = 2.0 Hz, 1H), 7.10 (d, *J* = 1.8 Hz, 1H), 7.07 (dd, *J* = 7.9, 1.8 Hz, 1H), 6.98 (d, *J* = 8.2 Hz, 1H), 6.91 (d, *J* = 7.9 Hz, 1H), 6.00 (s, 2H), 3.94 (s, 3H), 3.93 (s, 3H). MS (EI+) *m/z* calcd for C₂₂H₁₈N₂O₄ [M + H]⁺, 375.1; found, 375.2.

5-(2,4-Dimethoxyphenyl)-3-(3,4-dimethoxyphenyl)-1H-pyrrolo[2,3-b]pyridine (36). Compound 36 was prepared (86.2 mg, 74%) according to GP II (EtOAc/hexanes, gradient 1:3 to 1:1) from 5-bromo-3-(3,4-dimethoxyphenyl)-1H-pyrrolo[2,3-b]pyridine (100 mg, 0.3 mmol) and 2,4-dimethoxyphenyl boronic acid (65.5 mg, 0.36 mmol). ¹H NMR (300 MHz, chloroform-*d*) δ 9.94 (s, 1H), 8.48 (s, 1H), 8.28 (s, 1H), 7.46 (s, 1H), 7.28 (d, *J* = 8.8 Hz, 1H), 7.19 (dd, *J* = 8.2, 2.0 Hz, 1H), 7.16 (d, *J* = 2.0 Hz, 1H), 6.95 (d, *J* = 8.2 Hz, 1H), 6.61–6.59 (m, 2H), 3.93 (s, 3H), 3.91 (s, 3H), 3.86 (s, 3H), 3.80 (s, 3H). MS (EI+) *m/z* calcd for C₂₃H₂₂N₂O₄ [M + H]⁺, 391.2; found, 391.2.

4-(3-(3,4-Dimethoxyphenyl)-1H-pyrrolo[2,3-b]pyridin-5-yl)aniline (37). Compound 37 was prepared (29.3 mg, 57%) according to GP II (EtOAc/hexanes, gradient 1:1 to 3:1) from 5-bromo-3-(3,4-dimethoxy-

phenyl)-1H-pyrrolo[2,3-b]pyridine (50 mg, 0.15 mmol) and 4-(4,4,5,5-tetramethyl-1,3,2-dioxaborolan-2-yl)aniline (39.5 mg, 0.18 mmol) as yellow solid. ¹H NMR (400 MHz, DMSO-*d*₆) δ 11.76 (s, 1H), 8.44 (d, *J* = 2.1 Hz, 1H), 8.23 (d, *J* = 2.1 Hz, 1H), 7.77 (s, 1H), 7.41 (d, *J* = 8.5 Hz, 2H), 7.28 (dd, *J* = 8.2, 2.0 Hz, 1H), 7.25 (d, *J* = 2.0 Hz, 1H), 7.02 (d, *J* = 8.2 Hz, 1H), 6.68 (d, *J* = 8.5 Hz, 2H), 5.16 (s, 2H), 3.85 (s, 3H), 3.78 (s, 3H). ¹³C NMR (100 MHz, DMSO-*d*₆) δ 149.2, 147.9, 147.9, 147.2, 141.3, 129.4, 128.0, 127.5, 126.4, 123.8, 123.5, 118.6, 117.4, 114.5, 114.4, 112.5, 110.6, 55.6, 55.6. HRMS (EI+) *m/z* calcd for C₂₁H₁₉N₃O₂ [M + H]⁺, 346.1556; found, 346.1534.

5-(3-(3,4-Dimethoxyphenyl)-1H-pyrrolo[2,3-b]pyridin-5-yl)-pyrimidin-2-amine (38). Compound 38 was prepared (30.2 mg, 29%) according to GP II (EtOAc/hexanes, gradient 1:3 to 1:1) from 5-bromo-3-(3,4-dimethoxyphenyl)-1H-pyrrolo[2,3-b]pyridine (101.6 mg, 0.305 mmol) and (4,4,5,5-tetramethyl-1,3,2-dioxaborolan-2-yl)-pyrimidin-2-amine (74.2 mg, 0.335 mmol). ¹H NMR (400 MHz, DMSO-*d*₆) δ 11.90 (s, 1H), 8.63 (s, 2H), 8.46 (d, *J* = 2.0 Hz, 1H), 8.33 (d, *J* = 2.0 Hz, 1H), 7.82 (s, 1H), 7.31 (dd, *J* = 8.2, 2.1 Hz, 1H), 7.26 (d, *J* = 2.1 Hz, 1H), 7.01 (d, *J* = 8.2 Hz, 1H), 6.71 (s, 2H), 3.84 (s, 3H), 3.77 (s, 3H). MS (EI+) *m/z* calcd for C₁₉H₁₇N₅O₂ [M + H]⁺, 348.1; found, 348.2.

3-(3-(3,4-Dimethoxyphenyl)-1H-pyrrolo[2,3-b]pyridin-5-yl)-5-methoxyaniline (39). Compound 39 was prepared (40.8 mg, 36%) according to GP II (EtOAc/hexanes, 3:1) from 5-bromo-3-(3,4-dimethoxyphenyl)-1H-pyrrolo[2,3-b]pyridine (100 mg, 0.3 mmol) and 3-methoxy-5-(4,4,5,5-tetramethyl-1,3,2-dioxaborolan-2-yl)aniline (89.7 mg, 0.36 mmol) as white solid. ¹H NMR (400 MHz, DMSO-*d*₆) δ 11.86 (s, 1H), 8.47 (d, *J* = 2.1 Hz, 1H), 8.27 (d, *J* = 2.1 Hz, 1H), 7.81 (s, 1H), 7.28–7.26 (m, 2H), 7.04 (d, *J* = 8.8 Hz, 1H), 6.51 (s, 1H), 6.44 (s, 1H), 6.16 (s, 1H), 5.19 (s, 2H), 3.85 (s, 3H), 3.78 (s, 3H), 3.73 (s, 3H). ¹³C NMR (100 MHz, DMSO-*d*₆) δ 160.8, 150.3, 149.2, 148.5, 147.3, 141.7, 140.6, 129.4, 127.8, 124.9, 123.8, 118.6, 117.3, 114.7, 112.5, 110.7, 105.6, 100.7, 98.2, 55.6, 55.6, 54.7. HRMS (EI+) *m/z* calcd for C₂₂H₂₁N₃O₃ [M + H]⁺, 376.1661; found, 376.1643.

General Procedure (GP III) for Suzuki Coupling. **5-(3-(3,4-Dimethoxyphenyl)-1H-pyrrolo[2,3-b]pyridin-5-yl)-2-(2-morpholinoethoxy)aniline (40).** A solution of 47 (35 mg, 0.092 mmol), 5-bromo-2-(2-morpholinoethoxy)aniline (33 mg, 0.11 mmol), Cs₂CO₃ (60 mg, 0.184 mmol), and PdCl₂(dppf)·CH₂Cl₂ (18.8 mg, 0.023 mmol) in 1,4-dioxane/H₂O = 3:1 (1.5 mL) was charged in capped tube and was heated to 100 °C for 3 h. The reaction mixture was cooled to room temperature and concentrated in vacuo. The residue was diluted with CH₂Cl₂ and organic phase was extracted with CH₂Cl₂. The combined organic layer was dried with MgSO₄ and concentrated in vacuo. The mixture was purified with flash column chromatography (CH₂Cl₂/MeOH, gradient 30:1 to 15:1) to give the product, compound 40 as white solid (12.9 mg, 30%). ¹H NMR (400 MHz, chloroform-*d*) δ 9.48 (s, 1H), 8.52 (s, 1H), 8.27 (s, 1H), 7.44 (s, 1H), 7.20 (dd, *J* = 8.2, 2.0 Hz, 1H), 7.12 (d, *J* = 2.0 Hz, 1H), 6.98–6.88 (m, 4H), 4.17 (t, *J* = 5.6 Hz, 2H), 3.94 (s, 3H), 3.92 (s, 3H), 3.73 (t, *J* = 4.6 Hz, 4H), 2.82 (t, *J* = 5.6 Hz, 2H), 2.59 (t, *J* = 4.6 Hz, 4H). ¹³C NMR (150 MHz, chloroform-*d*) δ 149.4, 148.2, 148.0, 145.9, 142.8, 137.4, 133.4, 130.4, 127.7, 126.2, 121.8, 119.7, 118.4, 117.4, 116.9, 114.3, 113.3, 111.9, 110.9, 67.0, 66.8, 57.8, 56.1, 56.1, 54.0. HRMS (EI+) *m/z* calcd for C₂₇H₃₀N₄O₄ [M + H]⁺, 475.2345; found, 475.2350.

3-(3-(3,4-Dimethoxyphenyl)-5-(3-methoxyphenyl)-1H-pyrrolo[2,3-b]pyridine (41). Compound 41 was prepared (5.4 mg, 23%) according to GP I (EtOAc/hexanes, 1:1) from 5-bromo-3-iodo-1-(phenylsulfonyl)-1H-pyrrolo[2,3-b]pyridine (77.5 mg, 0.233 mmol) and 3-methoxyphenyl boronic acid (42.5 mg, 0.28 mmol). ¹H NMR (400 MHz, chloroform-*d*) δ 9.61 (s, 1H), 8.38 (s, 1H), 7.48 (s, 1H), 7.39 (t, *J* = 7.9 Hz, 1H), 7.24 (s, 1H), 7.23–7.16 (m, 2H), 7.14–7.09 (m, 2H), 6.98 (d, *J* = 8.3 Hz, 1H), 6.92 (dd, *J* = 8.3, 2.5 Hz, 1H), 3.94 (s, 3H), 3.93 (s, 3H), 3.87 (s, 3H). MS (EI+) *m/z* calcd for C₂₂H₂₀N₂O₃ [M + H]⁺, 361.2; found, 361.2.

■ ASSOCIATED CONTENT

Supporting Information

Spectra, rescoring of the generated 7-azaindole derivatives, kinase selectivity profiling, and physicochemical properties predicted by Accelrys DB. This material is available free of charge via the Internet at <http://pubs.acs.org>.

■ AUTHOR INFORMATION

Corresponding Authors

*For S.H.: phone, (+82) 42-350-2811; fax, (+82) 42-350-2810; E-mail, hongorg@kaist.ac.kr.

*For S.-S.-H.: phone, (+82) 32-890-3683; fax, (+82) 32-890-2462; E-mail, hong@s@inha.ac.kr.

Notes

The authors declare no competing financial interest.

■ ACKNOWLEDGMENTS

This research was supported by National Research Foundation of Korea (NRF) through general research grants (NRF-2011-0020322, Medical Research Center (2014009392)) and the Institute for Basic Science (IBS-R010-G1).

■ ABBREVIATIONS USED

SCF, stem cell factor; c-Kit, receptor tyrosine kinase for the stem cell factor; PI3K, phosphatidylinositol-3-kinase; Akt, known as protein kinase B (PKB); MAP kinase, mitogen-activated protein kinase; JAK, Janus-activated kinase; STAT, signal transducer and activator of transcription; SRC, a nonreceptor protein tyrosine kinase protein that in humans is encoded by the SRC gene; SFK, Src family kinase; GISTs, gastrointestinal stromal tumors; AML, acute myeloid leukemia; SM, systemic mastocytosis; WT, wild-type; ATP, adenosine-5'-triphosphate; A-loop, activation loop; SAR, structure–activity relationship; DFG, Asp-Phe-Gly; ADP, adenosine diphosphate; PDB, Protein Data Bank; POC, percent of control; IC₅₀, half-maximal inhibitory concentration; Erk, extracellular signal-regulated kinase; MTT, 3-(4,5-dimethylthiazol-2-yl)-2,5-diphenyltetrazolium bromide; TUNEL, terminal deoxynucleotidyl transferase-mediated nick end labeling; tPSA, topological polar surface area

■ REFERENCES

- (1) Kitamura, Y.; Hirotab, S. Kit as a human oncogenic tyrosine kinase. *Cell. Mol. Life Sci.* **2004**, *61*, 2924–2931.
- (2) (a) Blume Jensen, P.; Claesson Welsh, L.; Siegbahn, A.; Zsebo, K. M.; Westermarck, B.; Heldin, C. H. Activation of the human c-kit product by ligand-induced dimerization mediates circular actin reorganization and chemotaxis. *EMBO J.* **1991**, *10*, 4121–4128. (b) Ronnstrand, L. Signal transduction via the stem cell factor receptor/c-kit. *Cell. Mol. Life Sci.* **2004**, *2535*–2548.
- (3) (a) Blume Jensen, P.; Janknecht, R.; Hunter, T. The kit receptor promotes cell survival via activation of PI 3-kinase and subsequent Akt-mediated phosphorylation of Bad on Ser136. *Curr. Biol.* **1998**, *8*, 779–782. (b) Masson, K.; Ronnstrand, L. Oncogenic signaling from the hematopoietic growth factor receptors c-Kit and Flt3. *Cell Signal.* **2009**, *21*, 1717–1726.
- (4) (a) Kemmer, K.; Corless, C. L.; Fletcher, J. A.; McGreevey, L.; Haley, A.; Griffith, D.; Cummings, O. W.; Wait, C.; Town, A.; Heinrich, M. C. KIT mutations are common in testicular seminomas. *Am. J. Pathol.* **2004**, *164*, 305–313. (b) Heinrich, M. C.; Blanke, C. D.; Druker, B. J.; Corless, C. L. Inhibition of KIT tyrosine kinase activity: a novel molecular approach to the treatment of KIT-positive malignancies. *J. Clin. Oncol.* **2002**, *20*, 1692–1703. (c) Nagata, H.; Worobec, A. S.; Oh, C. K.; Chowdhury, B. A.; Tannenbaum, S.;

Suzuki, Y.; Metcalfe, D. D. Identification of a point mutation in the catalytic domain of the protooncogene c-kit in peripheral blood mononuclear cells of patients who have mastocytosis with an associated hematologic disorder. *Proc. Natl. Acad. Sci. U. S. A.* **1995**, *92*, 10560–10564.

(5) Heinrich, M.; Griffith, D.; Druker, B.; Wait, C.; Ott, K.; Ziegler, A. Inhibition of c-kit receptor tyrosine kinase activity by STI 571, a selective tyrosine kinase inhibitor. *Blood* **2000**, *96*, 925–932.

(6) Demetri, G. D.; von Mehren, M.; Blanke, C. D.; van den Abbeele, A. D.; Eisenberg, B.; Roberts, P. J.; Heinrich, M. C.; Tuveson, D. A.; Singer, S.; Janicek, M.; Fletcher, J. A.; Silverman, S. G.; Silberman, S. L.; Capdeville, R.; Kiese, B.; Peng, B.; Dimitrijevic, S.; Druker, B. J.; Corless, C.; Fletcher, C. D.; Joensuu, H. Efficacy and safety of imatinib mesylate in advanced gastrointestinal stromal tumors. *N. Engl. J. Med.* **2002**, *347*, 472–480.

(7) (a) Mol, C. D.; Lim, K. B.; Sridhar, V.; Zou, H.; Chien, E. Y.; Sang, B. C.; Nowakowski, J.; Kassel, D. B.; Cronin, C. N.; McRee, D. E. Structure of a KIT product complex reveals the basis for kinase transactivation. *J. Biol. Chem.* **2003**, *278*, 31461–31464. (b) Mol, C. D.; Dougan, D. R.; Schneider, T. R.; Skene, R. J.; Kraus, M. L.; Scheibe, D. N.; Snell, G. P.; Zou, H.; Sang, B. C.; Wilson, K. P. Structural basis for the autoinhibition and STI-571 inhibition of c-Kit tyrosine kinase. *J. Biol. Chem.* **2004**, *279*, 31655–31663.

(8) (a) Heinrich, M. C.; Corless, C. L.; Blanke, C. D.; Demetri, G. D.; Joensuu, H.; Roberts, P. J.; Eisenberg, B. L.; von Mehren, M.; Fletcher, C. D.; Sandau, K.; McDougall, K.; Ou, W. B.; Chen, C. J.; Fletcher, J. A. Molecular correlates of imatinib resistance in gastrointestinal stromal tumors. *J. Clin. Oncol.* **2006**, *24*, 764–774. (b) Lasota, J.; Corless, C. L.; Heinrich, M. C.; Debiec Rychter, M.; Sciort, R.; Wardelmann, E.; Merkelbach Bruse, S.; Schildhaus, H. U.; Steigen, S. E.; Stachura, J.; Wozniak, A.; Antonescu, C.; Daum, O.; Martin, J.; Del Muro, J. G.; Miettinen, M. Clinicopathologic profile of gastrointestinal stromal tumors (GISTs) with primary KIT exon 13 or exon 17 mutations: a multicenter study on 54 cases. *Mod. Pathol.* **2008**, *21*, 476–484.

(9) Longley, B. J., Jr.; Metcalfe, D. D.; Sharp, M.; Wang, X.; Tyrrell, L.; Lu, S. Z.; Heitjan, D.; Ma, Y. Activating and dominant inactivating c-KIT catalytic domain mutations in distinct clinical forms of human mastocytosis. *Proc. Natl. Acad. Sci. U. S. A.* **1999**, *96*, 1609–1614.

(10) Pardanani, A.; Akin, C.; Valent, P. Pathogenesis, clinical features, and treatment advances in mastocytosis. *Best Pract. Res. Clin. Haematol.* **2006**, *19*, 595–615.

(11) Longley, B. J.; Tyrrell, L.; Lu, S. Z.; Ma, Y. S.; Langley, K.; Ding, T. G.; Duffy, T.; Jacobs, P.; Tang, L. H.; Modlin, I. Somatic c-KIT activating mutation in urticarial pigmentosa and aggressive mastocytosis: establishment of clonality in a human mast cell neoplasm. *Nature Genet.* **1996**, *12*, 312–314.

(12) Bodemer, C.; Hermine, O.; Palmérini, F.; Yang, Y.; Grandpeix Guyodo, C.; Leventhal, P. S.; Hadj Rabia, S.; Nasca, L.; Georgin Lavalie, S.; Cohen Akenine, A.; Launay, J. M.; Barete, S.; Feger, F.; Arock, M.; Catteau, B.; Sans, B.; Stalder, J. F.; Skowron, F.; Thomas, L.; Lorette, G.; Plantin, P.; Bordigoni, P.; Lortholary, O.; de Prost, Y.; Moussy, A.; Sobol, H.; Dubreuil, P. Pediatric mastocytosis is a clonal disease associated with D816V and other activating c-KIT mutations. *J. Invest. Dermatol.* **2010**, *130*, 804–815.

(13) (a) Gajiwala, K. S.; Wu, J. C.; Christensen, J.; Deshmukh, G. D.; Diehl, W.; DiNitto, J. P.; English, J. M.; Greig, M. J.; He, Y. A.; Jacques, S. L.; Lunney, E. A.; McTigue, M.; Molina, D.; Quenzer, T.; Wells, P. A.; Yu, X.; Zhang, Y.; Zou, A.; Emmett, M. R.; Marshall, A. G.; Zhang, H. M.; Demetri, G. D. KIT kinase mutants show unique mechanisms of drug resistance to imatinib and sunitinib in gastrointestinal stromal tumor patients. *Proc. Natl. Acad. Sci. U. S. A.* **2009**, *106*, 1542–1547. (b) Frost, M. J.; Ferrao, P. T.; Hughes, T. P.; Ashman, L. K. Juxtamembrane mutant V560G Kit is more sensitive to Imatinib (STI571) compared with wild-type c-kit whereas the kinase domain mutant D816V Kit is resistant. *Mol. Cancer Ther.* **2002**, *1*, 1115–1124.

(14) Shah, N. P.; Lee, F. Y.; Luo, R.; Jiang, Y.; Donker, M.; Akin, C. Dasatinib (BMS-354825) inhibits KITD816V, an imatinib-resistant

activating mutation that triggers neoplastic growth in most patients with systemic mastocytosis. *Blood* **2006**, *108*, 286–291.

(15) Lierman, E.; Smits, S.; Cools, J.; Dewaele, B.; Debiec Rychter, M.; Vandenberghe, P. Ponatinib is active against imatinib-resistant mutants of FIP1L1-PDGFR α and KIT, and against FGFR1-derived fusion kinases. *Leukemia* **2012**, *26*, 1693–1695.

(16) (a) Knight, Z. A.; Shokat, K. M. Features of selective kinase inhibitors. *Chem. Biol.* **2005**, *12*, 621–637. (b) Smyth, L. A.; Collins, I. Measuring and interpreting the selectivity of protein kinase inhibitors. *J. Chem. Biol.* **2009**, *2*, 131–151. (c) Hasinoff, B. B.; Patel, D.; O'Hara, K. A. Mechanisms of myocyte cytotoxicity induced by the multiple receptor tyrosine kinase inhibitor sunitinib. *Mol. Pharmacol.* **2008**, *74*, 1722–1728. (d) Zhang, X.; Crespo, A.; Fernández, A. Turning promiscuous kinase inhibitors into safer drugs. *Trends Biotechnol.* **2008**, *26*, 295–301. (e) Verheul, H. M.; Pinedo, H. M. Possible molecular mechanisms involved in the toxicity of angiogenesis inhibition. *Nature Rev. Cancer* **2007**, *7*, 475–485.

(17) Fabian, M. A.; Biggs, W. H.; Treiber, D. K.; Atteridge, C. E.; Azimioara, M. D.; Bendetti, M. G.; Carter, T. A.; Ciceri, P.; Edeen, P. T.; Floyd, M.; Ford, J. M.; Galvin, M.; Gerlach, J. L.; Grotzfeld, R. M.; Herrgard, S.; Insko, D. E.; Insko, M. A.; Lai, A. G.; Lelias, J.-M.; Mehta, S. A.; Milanov, Z. V.; Velasco, A. M.; Wodicka, L. M.; Patel, H. K.; Zarrinkar, P. P.; Lockhart, D. J. A small molecule–kinase interaction map for clinical kinase inhibitors. *Nature Biotechnol.* **2005**, *23*, 329–336.

(18) (a) Hong, S.; Lee, S.; Kim, B.; Lee, H.; Hong, S.-S.; Hong, S. Discovery of new azaindole-based PI3K α inhibitors: apoptotic and antiangiogenic effect on cancer cells. *Bioorg. Med. Chem. Lett.* **2010**, *20*, 7212–7215. (b) Hong, S.; Kim, J.; Seo, J.; Jung, K.; Hong, S.-S.; Hong, S. Design, synthesis and evaluation of 3,5-disubstituted 7-azaindoles as Trk inhibitors with anticancer and anti-angiogenic activities. *J. Med. Chem.* **2012**, *55*, 5337–5349.

(19) Knight, S. D.; Adams, N. D.; Burgess, J. L.; Chaudhari, A. M.; Darcy, M. G.; Donatelli, C. A.; Luengo, J. I.; Newlander, K. A.; Parrish, C. A.; Ridgers, L. H.; Sarpong, M. A.; Schmidt, S. J.; Van Aller, G. S.; Carson, J. D.; Diamond, M. A.; Elkins, P. A.; Gardiner, C. M.; Garver, E.; Gilbert, S. A.; Gontarek, R. R.; Jackson, J. R.; Kershner, K. L.; Luo, L.; Raha, K.; Sherk, C. S.; Sung, C. M.; Sutton, D.; Tummino, P. J.; Wegrzyn, R. J.; Auger, K. R.; Dhanak, D. Discovery of GSK2126458, a highly potent inhibitor of PI3K and the mammalian target of rapamycin. *ACS Med. Chem. Lett.* **2010**, *1*, 39–43.

(20) (a) Hong, S.; Kim, J.; Seo, J. H.; Jung, K. H.; Hong, S. S.; Hong, S. Design and synthesis of imidazopyridine analogues as inhibitors of phosphoinositide 3-kinase signaling and angiogenesis. *J. Med. Chem.* **2011**, *54*, 2455–2466. (b) Hong, S.; Kim, J.; Seo, J. H.; Jung, K. H.; Hong, S. S.; Hong, S. Selectivity enhancement arising from interactions at the PI3K unique pocket. *ChemMedChem* **2012**, *7*, 1379–1383. (c) Jeong, Y.; Kwon, D.; Hong, S. Selective and Potent Small-Molecule Inhibitors of Phosphatidylinositol 3-Kinases. *Future Med. Chem.* **2014**, *6*, 737–756.

(21) Vendôme, J.; Letard, S.; Martin, F.; Svinarchuk, F.; Dubreuil, P.; Auclair, C.; Le Bret, M. Molecular modeling of wild-type and D816V c-Kit inhibition based on ATP-competitive binding of ellipticine derivatives to tyrosine kinases. *J. Med. Chem.* **2005**, *48*, 6194–6201.

(22) Mol, C. D.; Lim, K. B.; Sridhar, V.; Zou, H.; Chien, E. Y.; Sang, B. C.; Nowakowski, J.; Kassel, D. B.; Cronin, C. N.; McRee, D. E. Structure of a c-Kit product complex reveals the basis for kinase transactivation. *J. Biol. Chem.* **2003**, *278*, 31461–31464.

(23) Nolen, B.; Taylor, S.; Ghosh, G. Regulation of protein kinases: controlling activity through activation segment conformation. *Mol. Cell* **2004**, *15*, 661–675.

(24) Wang, R.; Gao, Y.; Lai, L. LigBuilder: a multi-purpose program for structure-based drug design. *J. Mol. Model.* **2000**, *6*, 498–516.

(25) Wang, R.; Liu, L.; Lai, L. SCORE: A new empirical method for estimating the binding affinity of a protein–ligand complex. *J. Mol. Model.* **1998**, *4*, 379–394.

(26) The IC₅₀ determinations were performed at the Reaction Biology Corp. (Malvern, PA, USA). POC determinations were performed at the Ambit Bioscience Corp. (San Diego, CA, USA).